Adv Biochem Engin/Biotechnol (2009) 116: 29–72
DOI: 10.1007/10_2008_9

Published online: 01 October 2008

Plasmon-Controlled Fluorescence Towards High-Sensitivity Optical Sensing

K. Ray, M. H. Chowdhury, J. Zhang, Y. Fu, H. Szmacinski, K. Nowaczyk, and J. R. Lakowicz

Abstract Fluorescence spectroscopy is widely used in chemical and biological research. Until recently most of the fluorescence experiments have been performed in the far-field regime. By far-field we imply at least several wavelengths from the fluorescent probe molecule. In recent years there has been growing interest in the interactions of fluorophores with metallic surfaces or particles. Near-field interactions are those occurring within a wavelength distance of an excited fluorophore. The spectral properties of fluorophores can dramatically be altered by near-field interactions with the electron clouds present in metals. These interactions modify the emission in ways not seen in classical fluorescence experiments. Fluorophores in the excited state can create plasmons that radiate into the far-field and fluorophores in the ground state can interact with and be excited by surface plasmons. These reciprocal interactions suggest that the novel optical absorption and scattering properties of metallic nanostructures can be used to control the decay rates, location, and direction of fluorophore emission. We refer to these phenomena as plasmon-controlled fluorescence (PCF). An overview of the recent work on metal—fluorophore interactions is presented. Recent research combining plasmonics and fluorescence suggest that PCF could lead to new classes of experimental procedures, novel probes, bioassays, and devices.

Keywords Fluorescence, Metal-enhanced fluorescence, Plasmon-controlled fluorescence, Sensing, Single molecule detection, Surface-plasmon coupled emission

K. Ray, M.H. Chowdhury, J. Zhang, Y. Fu, H. Szmainski, K. Nowaczyk, and J.R. Lakowicz (✉)
Center for Fluorescence Spectroscopy, Department of Biochemistry and Molecular Biology, University of Maryland School of Medicine, 725 W Lombard St, Baltimore, MD 21201, USA

Contents

1 Introduction

In recent years there has been growing interest in investigating the interactions of fluorophores with metallic surfaces or particles. Recent research from this laboratory has revealed a number of important effects, such as increases in intensity, photostability, and fluorescence resonance energy transfer (FRET) near metal particles and directional emission near planar metallic surfaces. We believe these effects will result in a new generation of methods, probes, and devices for the use of fluorescence in the biosciences. Because of the importance of these phenomena we have attempted to provide a summary of these effects to stimulate further research in this area. In classical fluorescence, all emission is detected as radiation propagating to the far-field. In contrast to far-field optics, the near-field effects are more complex. This chapter is intended to provide an overview of fluorophore–metal interactions, rather than an exhaustive review, and we apologize to authors for not citing all of their papers.

In general, almost all uses of fluorescence depend on the spontaneous emission of photons occurring nearly isotropically in all directions (Fig. 1). For this case, information about the sample is obtained primarily from changes in the nonradiative decay rates k_{nr}, such as collisions of fluorophores with quenchers k_q and fluorescence resonance energy transfer k_T. In classical fluorescence experiments the changes in quantum yields and lifetimes are caused by changes in the nonradiative decay rates k_{nr}, which result from changes in a fluorophore's environment, quenching, or FRET. The radiative decay rate Γ is essentially constant and any changes are primarily due to changes in refractive index. The values of Φ_0 and τ_0 either both increase or decrease, but do not change in opposite directions. The brightness and lifetime of a fluorophore also depend on the radiative decay rate Γ of the fluorophore. However, the rates of spontaneous emission of fluorophores are determined by their extinction coefficients [1] and are not significantly changed in most experiments.

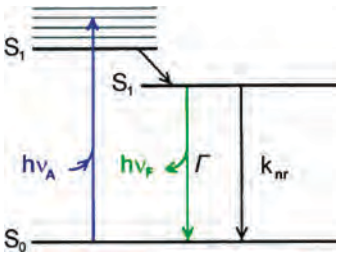

Fig. 1 Jablonski diagram

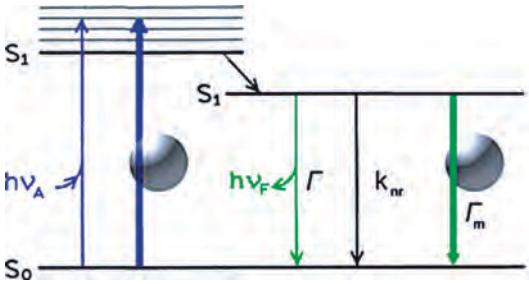

Fig. 2 Modified Jablonski diagram that includes metal–fluorophore interactions. The *thicker arrows* represent increased rates of excitation and emission

Metal colloids can interact strongly with incident light (Fig. 2). The optical cross-sections or extinction coefficients of metal colloids can be 10^5-times larger than for a fluorophore [2–3]. Because of these large optical cross-sections, metallic colloids are used as probes for biological imaging and sensing [4–5]. While the high optical cross-sections make the metal colloids valuable as scattering probes, the scattered light from both the colloid and the sample occur at the same wavelength as the incident light. The use of fluorophores near metal particles offers the opportunity to utilize the larger effective extinction coefficient of metal particles and the Stokes' shift of fluorescence. The local fields around the colloid due to incident light can result in increased excitation of fluorophores near the metals, which takes advantage of the large extinction coefficients of the colloids. Additionally, an excited state fluorophore can interact with a nearby metal colloid to create plasmons. The fluorophore-induced plasmons can radiate to the far-field and create observable emission [6]. This emission occurs rapidly and is the origin of the decreased lifetimes.

Because the emission spectra remain the same it is often unclear which species is emitting. Since the lifetimes are decreased, and plasmon decay rates are fast (a typical lifetime of about 50 fs), [7–8] it seems that the metal is emitting. However, the emission spectrum is the same as that of the fluorophore, suggesting that the fluorophore is the emitting species. Therefore, as the emission retains the same spectrum as the fluorophore, we consider the fluorophore–metal complex as the emitting species. This emission has properties of both the fluorophore and the metal. For this reason we refer to this emitting species as a plasmophore.

While we believe the emission is from the plasmophore, the effect of metals can be described from the perspective of the fluorophore. The quantum yield and lifetime of a fluorophore are interrelated as defined below [9–10]:

$$\Phi_0 = \frac{\Gamma}{\Gamma + k_{nr}} \tag{1}$$

$$\tau_0 = \frac{1}{\Gamma + k_{nr}} \tag{2}$$

where Γand k_{nr} are the radiative and nonradiative decay rates, respectively. In the presence of metal, the quantum yield and lifetime are given by

$$\Phi_m = \frac{\Gamma + \Gamma_m}{\Gamma + \Gamma_m + k'_{nr}} \tag{3}$$

$$\tau_m = \frac{1}{\Gamma + \Gamma_m + k'_{nr}} \tag{4}$$

where Γ_m and $k_{nr}{}'$ are radiative and nonradiative rates in the presence of metal particles. Increases in radiative rates near metal particles result in increased quantum yields and decreased lifetimes. The modifications of k_{nr} by metal are assumed to be negligible. The above equations result in the unusual prediction for fluorophore—metal interactions that the lifetime decreases as the intensity increases. A decrease in lifetime has several favorable consequences. Reduction in lifetime affords increased fluorophore photostability, as there is less time for excited state photodestructive processes to occur. Also, fluorophores can become less prone to optical saturation and have higher maximum emission rates. Thus, increase in emission intensity accompanied by a decrease in lifetime results in increased detectability of single or multiple fluorophores.

2 Types of Metal–Fluorophore Interactions

Although metal—fluorophore interactions are based on the same physical principles, the effects can be different based on the geometry of the metal structure. Figure 3 presents three possibilities: a fluorophore interacting with (1) metallic nanoparticles, (2) a smooth metal surface, and (3) a metal surface with a regular pattern. Metal particles can typically be used to increase the fluorescence intensities. This increase occurs by a combination of enhanced fields around the metal and rapid and efficient plasmophore emission. These effects are usually called metal-enhanced fluorescence (MEF, Fig. 3, top panel), and typically result in increased intensities and decreased lifetimes.

The lower left panel (Fig. 3) shows a fluorophore interacting with a smooth metal film, typically about 40-nm thick silver, gold or 20-nm thick aluminum films. In this

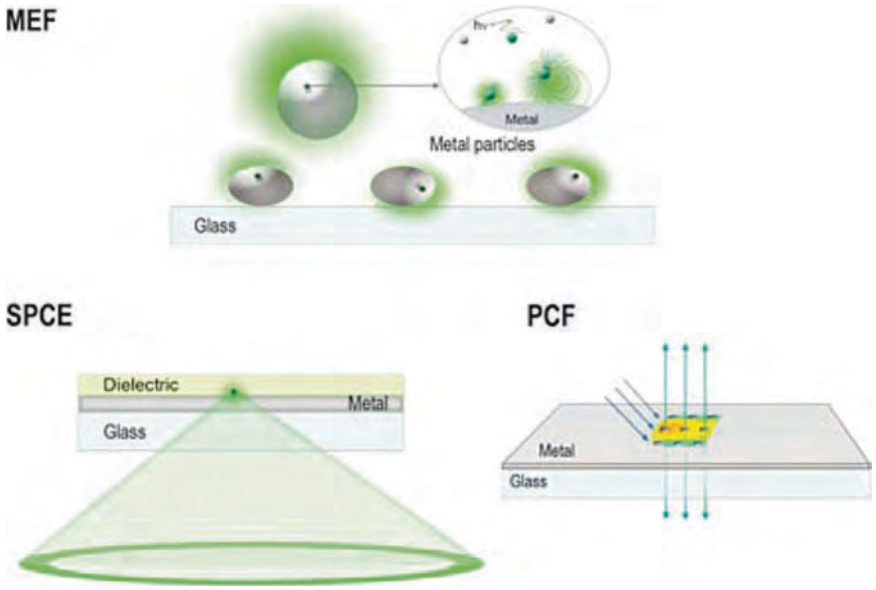

Fig. 3 Schematic representations of different types of metal–fluorophore interactions

case the fluorophore creates plasmons which radiate at a defined angle into the substrate. In general, the intensities and lifetimes are not dramatically changed. Surface plasmon-coupled emission (SPCE) is used to describe the directional light radiated into the underlying substrate when a fluorophore is near a continuous thin metal film [11–12]. We use the term SPCE because the emission spectrum is the same as the fluorophore but the polarization properties indicate the plasmon is radiating.

Figure 3 also shows a fluorophore above patterned metallic nanostructures. In this case the emission at certain wavelengths is expected to show well-defined beaming into the substrate, while other wavelengths are deflected from the normal. These effects are due to a combination of interactions with a smooth surface and with the sub-wavelength features. Plasmon-controlled fluorescence (PCF) is used to describe the more general case where a fluorophore is near a patterned metallic nanostructure, clusters of well-defined particle, or nanohole arrays. These three terms, MEF, SPCE, and PCF all refer to the interactions of fluorophores with metals, but it is easier to describe different types of experiments using different acronyms.

3 Experimental Studies of Fluorophore–Metal Interactions

Prior to 2000 there were a limited number of publications on the effects of metals or metallic nanostructures on fluorescence [13–18]. Since that time there has been rapid growth in the number of reports on metal—fluorophore interactions. In the

following section, we present some of the experimental results from our laboratory demonstrating the usefulness of fluorophore—metal interactions towards the biological applications of fluorescence.

4 Metal-Enhanced Fluorescence of Organic Fluorophores on Silver, Gold, and Aluminum Nanostructured Substrates

The general usefulness of MEF sensing can be expanded if MEF occurs with metals other than silver. Figure 4 shows the effects of MEF for a commonly used dye Cy5 in DNA microarrays. We have utilized MEF to increase the fluorescence yield of DNA microarrays by as much as 28-fold for the near infrared Cy5 dye [19]. This result demonstrates how MEF can be used to increase the sensitivity of DNA arrays, especially for far red emitting fluorophores like Cy5, without significantly altering current microarray protocols.

The electrodynamic nature of fluorophore–metal interaction caused us to consider other metals. For example, it is well-known that gold strongly quenches fluorescence [20–25]. However, from the optical constants of gold we reasoned that MEF and SPCE could occur at long wavelengths, above the intra band absorption of gold and this was found to occur. Gold is an attractive MEF substrate because of the high chemical stability of gold and its well developed and facile surface chemistry. Glass slides coated with gold particles were prepared by thermal vapor deposition. The absorption spectra showed that the evaporated films are particulate in nature (not shown). Figure 5 shows over sixfold increased intensities for AlexaFluor 555-labeled IgG. We believe we observed MEF rather than quenching for the following reasons. Gold particles thermally deposited on the surface were probably larger than those gold particle sizes reported for quenching [26–27]. Larger gold particles have more scattering than absorption in the optical extinction. MEF

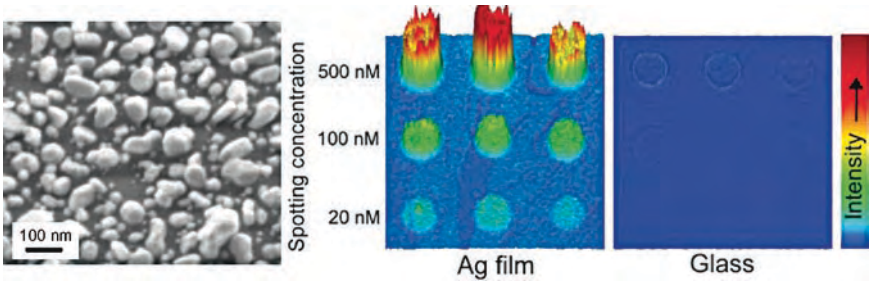

Fig. 4 (*Left panel*) Field emission scanning electron micrograph of the silver island film (SIF) showing the heterogeneity of the particles' shapes and sizes. (*Right panel*) Fluorescence image of labeled oligonucleotide targets hybridized to MEF and glass DNA arrays. Probe oligonucleotides (23mer) were arrayed onto the substrates at different spotting concentrations: each row represents replicate spots at a given concentration. The image shows the Cy5 fluorescence as a result of co-hybridization with complementary Cy5-labeled targets (23mer)

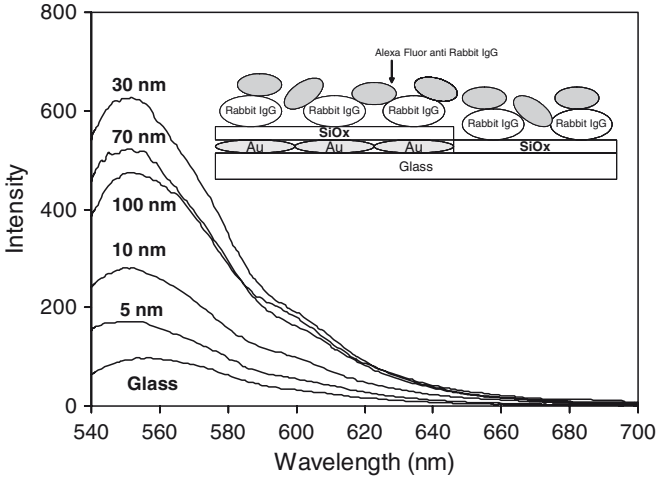

Fig. 5 Fluorescence spectra of Alexa Fluor-555 labeled anti-Rabbit IgG on varying thickness gold films upon excitation at 514 nm. All gold films were coated by 5 nm silica. *Insert* shows the schematic of the sample

observed using gold could also be due to the irregular particles formed by vapor deposition. Additionally, we separated the AlexaFluor 555-labeled IgG from the gold surfaces by a 5-nm coating of silica. Quenching by gold may occur at shorter distances and enhancement at larger distances above several nm. It is important to note that 5 nm silica is similar to the thickness of a monolayer of albumin or IgG, and that gold MEF occurs at distances that are useful in surface-bound assays. The observation of MEF using gold particles suggests the use of these stable particles in surface-localized bioassays. Although the enhancement observed with gold is less than that usually reported for the silver particles, the gold is chemically stable with well-defined surface chemistry, so that devices may be readily fabricated for long-term use.

Aluminum is also thought to quench fluorescence, but there are few reports on this effect [27]. Furthermore, aluminum surfaces are highly reactive and bare aluminum surfaces are quickly coated with an oxide. However, this process is self-limiting and does not continue after the oxide coating is formed. We knew that aluminum mirrors were useful in the UV, at shorter wavelengths than can be used with silver mirrors. Examination of the optical constants of aluminum showed that aluminum does not absorb light until the wavelengths are deep in the UV. We have examined if aluminum particles would be useful for MEF. Slides were coated with aluminum by vapor deposition. The particle size depended on the amount of aluminum on these surfaces. For 10-nm thick vapor deposited Al films, the particle sizes were about 100 nm, as shown in the SEM image (Fig. 6). We found significant enhancement in fluorescence intensity for 2-amino purine (2-AP) on aluminum nanostructures [28] (Fig. 6). Moreover, aluminum nanostructured substrates are very stable in buffers that contain chloride salts compared to the usual silver

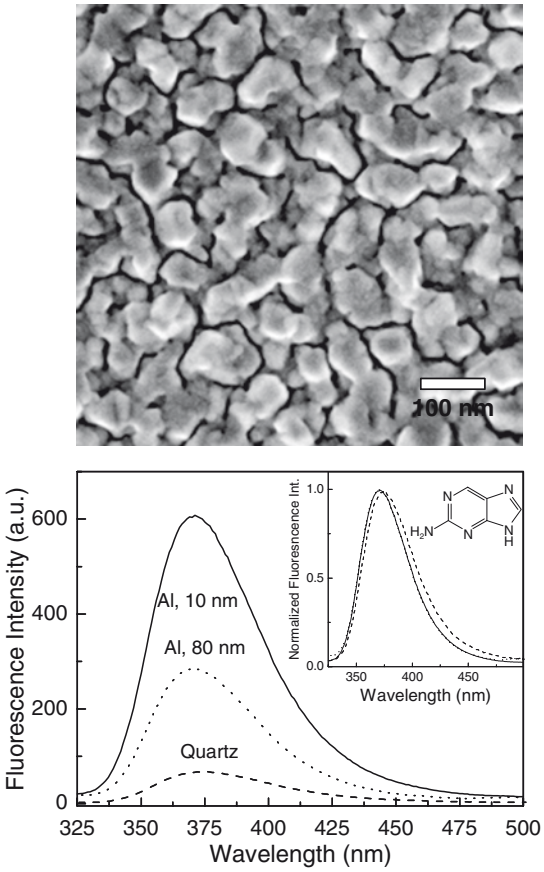

Fig. 6 (top) SEM image of evaporated 10-nm Al films. (bottom) Emission spectra of 2-AP on glass slides coated with aluminum particles

colloid-based substrates for MEF, thus furthering the usefulness of these aluminum-based substrates in many biological assays where high concentration of salts are required. Experimental results with silver, aluminum, and gold nanostructured substrates suggest that MEF can be observed with a wide range of fluorophores from the UV to the NIR regions of the spectra using a variety of metals.

5 Metal-Enhanced Fluorescence with Quantum Dots, Phycobiliproteins, and Lanthanides

Organic fluorophores are widely used for fluorescence sensing and imaging. However, MEF will become more valuable if it occurs with fluorophores other than small organic molecules. Semiconducting quantum dots (QDs) have been reported to possess numerous photophysical properties that are superior to those of organic

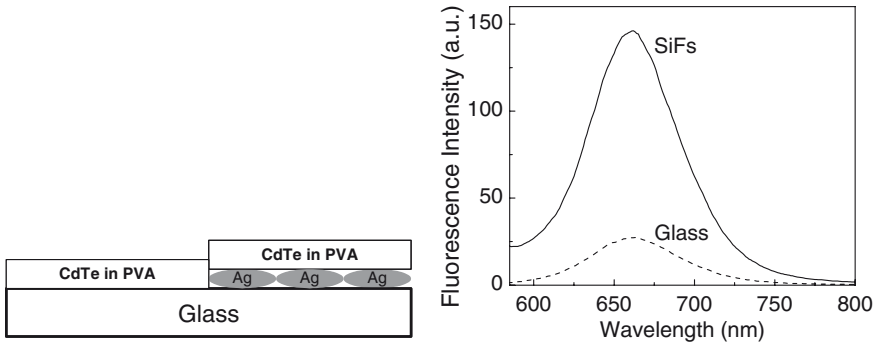

Fig. 7 Fluorescence spectra of CdTe nanocrystals on glass and SIF

fluorophores. The emission properties of quantum dots, especially high-absorption cross-section, exceptional photostability, wide excitation spectra and narrow emission bands, are important to live cell imaging and FRET biosensors.

Figure 7 shows the emission spectra of CdTe Qdots on glass and silver island films (SIFs), showing an approximate five-fold increase in intensity. We also observed a decrease in lifetime of the Q-dots on silver nanostructures [29]. These spectral changes suggest an increase in the radiative rate of the Qdots, which has been observed in other laboratories [30–31]. Phycobiliproteins have high fluorescence quantum yields, which are remarkably constant over broad pH range. Further enhancing the fluorescence emission properties and improving the photostability of phycobiliproteins will serve to make them even more efficient labels in the analysis of biomolecules and cells. This may be possible by utilizing the close-range (within 100 nm) interactions of these proteins with plasmonic nanoparticles. MEF has also been observed for several phycobiliproteins [32]. Figure 8 (left) shows emission spectra of cross-linked allophycocyanin (XAPC) on glass and silver island films. The increase in XAPC brightness is apparent from the real-color photographs on glass and silver nanostructures. We have also observed a decrease in lifetime for the XAPC molecules on the silver nanostructures as compared to the glass control as shown in Fig. 8. MEF observed with phycobiliproteins can be employed to increase the sensitivity of biological applications that employ phycobiliproteins as fluorescence labels such as flow cytometry, where biomolecules can flow through microchannels that are potentially coated with SIFs or other silver nanostructures, with no chemical linkage between the silver and the molecules.

We have also observed increases in emission intensities and decreased lifetimes for lanthanides near silver nanoparticles (not shown) [33–34]. Highly photostable long-lifetime lanthanide probes are very useful as these probes are suitable for off-gating biological autofluorescence. These results show that MEF occurs with all types of fluorophores, making MEF applicable to many types of assays. The fact that MEF occurs with all types of fluorophores is because MEF is due to a through-space interaction between the excited state dipole moment of the fluorophore and the metal surface. This is similar to FRET, which is also due to a through-space near-field interaction, and FRET also occurs with all types of fluorophores.

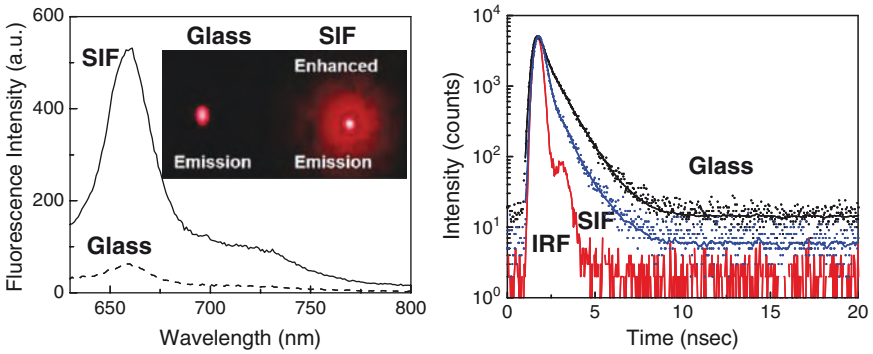

Fig. 8 Emission spectra, photograph (*left panel*), and lifetimes (*right panel*) of cross-linked allophycocyanin monolayer assembled on glass and silver island films

6 Association of Biomolecules in the Presence of Metal Nanoparticles

Since the early days of biochemical fluorescence there has been continued use of fluorophores that display spectral changes in response to a change in the local environment. Perhaps the most well-known probe of this type is 1-anilino-8-naphthalene sulfonic acid (ANS) and its derivatives [35–37]. These probes are weakly fluorescent in water but become highly fluorescent when bound to proteins or membranes. Similar probes exist for DNA, such as ethidium bromide, its dimers, and probes of the TOTO-YOYO series. These probes are weakly nonfluorescent in water and become highly fluorescent when bound to double helical DNA [38–40]. In many applications it is desirable to have the brightest possible probes which are covalently linked to the molecule of interest. Typical probes of this type are the rhodamines, cyanines, and Alexa probes. While these probes are bright they usually do not display significant changes in intensity in response to changes in their local environment. For instance, an Alexa-labeled protein may not change intensity upon binding to another protein, or a Cy5-labeled single strain of DNA may not change intensity upon hybridization with its complementary strand. Hence such probes are useful for tracking biomolecules, but are less useful for studies of functions.

Metal-enhanced fluorescence provides an opportunity to obtain changes in intensity upon a binding interaction for almost any fluorophore. The basic idea is to couple the binding reaction to proximity to a metal particle. One example is binding of a fluorescein-labeled DNA oligomer to a complementary strand [41]. This strand is bound to silver particles via a thiol group (Fig. 9). When the fluorescein-labeled DNA binds near the metal its intensity is increased, not by hybridization, but by proximity to the silver particles. As described above all types of fluorophores display MEF. Hence, MEF-based binding assays can be used to measure a large range of surface-bound assays.

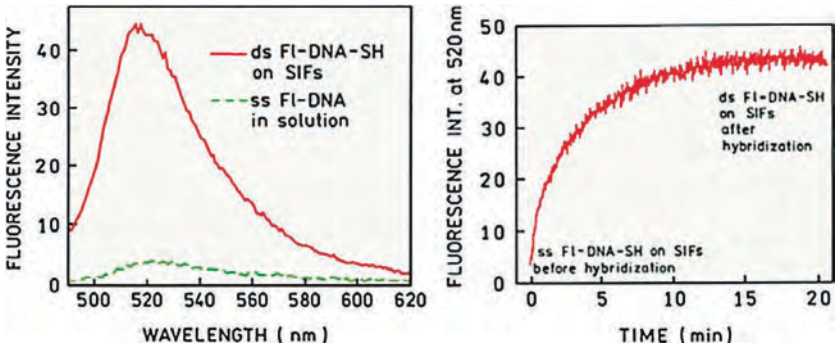

Fig. 9 Emission spectra and time-dependent intensity of a fluorescein-labeled oligomer upon binding to a complementary oligomer bound exclusively to a SIF. Reprinted with permission from Elsevier Science [41]

7 Synthesis and Characterization of Plasmon-Coupled Probes for Sensing

An important phenomenon in the development of plasmonic probes is the strong interaction of light with metallic particles. Suspensions of metallic colloids display brilliant colors that results from both absorption and scattering of light. The colors of colloids are not due to chromophores but rather to electron oscillations in the colloids induced by the incident light. The energy from the incident light is contained within the size of the colloids plus the space occupied by the surrounding evanescent field. The energy contained in these oscillations is dissipated either by dipole radiation into the far-field or by conversion into heat. These mechanisms account for the scattering and absorption components of the colloids extinction, respectively. Combination of plasmonic nanostructures and fluorescence provides an opportunity to create ultra-bright probes based on the interactions of metal particles with fluorophores. The basic idea is to create metal-conjugated fluorophore particles in which the metal particles amplify the brightness of the bound fluorophores. This can be achieved by trapping the fluorophores inside metal shells or by coating metal nanoparticles with fluorophores.

Recent theoretical calculations have shown that a fluorophore in metal shells can be 100-fold brighter than the isolated fluorophore, even after consideration of the transfer efficiency of incident light into the shell and radiation out of the shell [42–43]. Figure 10 shows an example of a plasmon-coupled probe where $Ru(bpy)^{2+}_3$ was adsorbed inside silica nanoparticles. The silver shell was coated onto the silica bead layer by layer through a chemical reduction of silver nitrate using sodium citrate in water. The emission spectrum became narrow relative to the bare bead when the metal shell was 20 nm and the emission intensity was enhanced with an increase of shell thickness, which was consistent with the theoretical predictions for the metal shells. The emission enhancement reached saturation at a thickness of 40 nm and then decreased probably due to the absorption from the metal shell at wave-

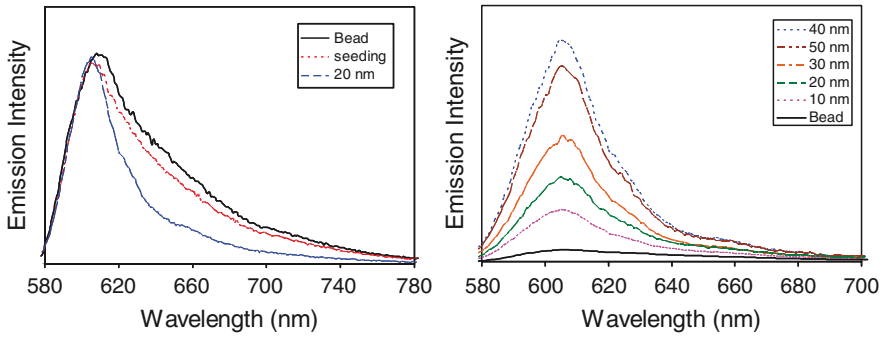

Fig. 10 Emission spectra of a silica bead containing $Ru(bpy)_3^{2+}$ alone and coated with 20-nm silver shell (*left panel*). Effect of increasing thickness of silver shells on silica bead with $Ru(bpy)_3^{2+}$ (*right panel*). Revised and reprinted with permission from American Chemical Society [44]

lengths of excitation and emission of the dye [44]. Such probes may have an advantage over quantum dots because of the low toxicity of silver particles, even if the silver surface is completely exposed. In contrast, quantum dots require a surface coating to avoid exposure of the toxic metal cadmium. The lifetime of $Ru(bpy)^{2+}_3$ in the silica bead is also shorter with an increase of silver shell thickness, which might be due to an increase of the intrinsic decay rate for the fluorophore near the metal surface. These nanoparticles show considerable promise for markers in biological sensing.

Figure 11 shows an example where silver colloids are coated with two different fluorophores, europium chelate and rhodamine 800. These probes are made from a silver core, and a silica shell with fluorophores embedded within the silica shell. A several-fold increase in brightness was observed for both fluorophores [45–46].

8 Metal-Enhanced Fluorescence: Phase-Modulation Fluorometry for Sensing

Fluorescence-based methods are widely used in studies of biomolecular interactions due to the availability of fluorescent materials, established labeling procedures, and sensitive detection. Higher sensitivity detection and more facile sample preparation and operating procedures are always in great demand in the biomedical and biotechnology fields. The area of particular interest is further development of fluoroimmunoassays which are generally based on an antibody-antigen binding event [47–49]. Perhaps the most well-known example of fluoroimmunoassays is sandwich-based enzyme-linked immunosorbent assays (ELISA) [50]. The ELISA is regarded as one of the most sensitive techniques for detection of interacting biomolecules because of enzymatic amplification of the signal but it requires a multistep procedure.

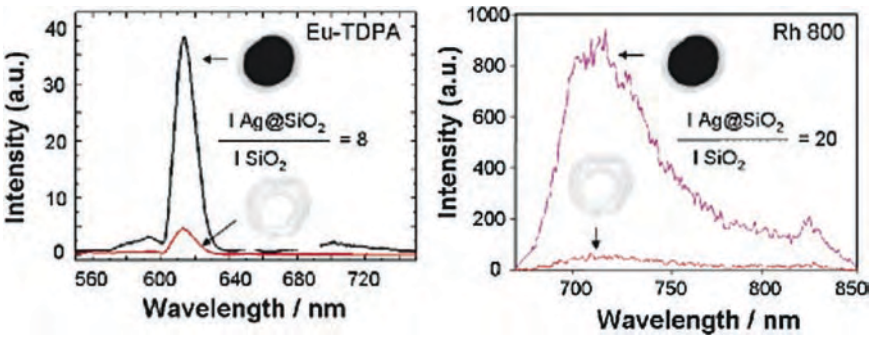

Fig. 11 Fluorescence intensity of Eu-TDPA-doped Ag@SiO_2 and Rh880-doped Ag@SiO_2, and from the corresponding fluorescent nanobubbles with silver removed (control samples), Eu-TDPA-doped SiO_2, and Rh800-doped SiO_2. *Inset*: TEM images of Ag@SiO_2nanoballs. The diameter of the Ag is 130 ± 10 nm and the thickness of the shell is 11 ± 1 nm as measured by TEM. Reprinted with permission from the American Chemical Society [46]

Herein we describe a new assay design approach that incorporates both of the effects of MEF, fluorescence intensity amplification and lifetime reduction, in combination with phase-modulation (PM) fluorometry. This new technique (MEF-PM) allows ultra-sensitive detection, simplified sample preparation procedure, and the possibility of real-time monitoring of biomolecular interactions. MEF-PM utilizes the large contrast in the lifetime and intensity between bound and unbound reporter antibodies that allows measurement of the analyte concentration without the washing steps necessary for conventional fluoroimmunoassays. The quantification of IgG_3 produced during cell culture has been chosen as an example of demonstrating the MEF-PM capabilities to a sandwich-based fluoroimmunoassay typically used for ELISA analysis [51].

Figure 12 shows the schematic of the MEF-PM measurements in comparison to a standard surface-based assay on a glass substrate including the ELISA format, where washing out unbound probes is required prior to the intensity readout. The standard assays are mostly intensity-based immunoassays for detection of the analyte concentration present in clinical and biological samples. Typically, the intensity-based approach of surface-based fluoroimmunoassays requires that any unbound probe be removed prior to signal readout. This is largely for two reasons: (1) the bound fluorescent probe usually has similar fluorescent properties compared to those of the free probe and (2) there is usually a large excess of the free probes compared to that of the bound probes. As a result, a washing step is required before readout. When biomolecule interaction occurs on the MEF substrates, a large intensity enhancement of the bound probes in comparison to the free probes allows the detection of intensity changes in the presence of the free probes. This is shown in Fig. 13 where the fluorescence intensity-based calibration curves were generated using a capture antibody (goat anti-mouse IgG_3) and standard antigen IgG_3 (Pharmingen) and serial dilution. Following antigen binding, the reporter antibody labeled with Cy5 (IgG_3-Cy5) was added and allowed to incubate for 1 h at room

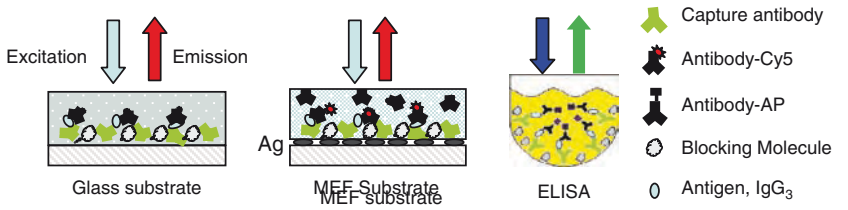

Fig. 12 Schematics of sandwich assays for the detection of IgG3 on glass, MEF substrates (silver island film), and using ELISA. Note that detection of IgG_3 on glass and using ELISA requires washing out the unbound probes while on MEF substrates. The readout is in the presence of unbound probes

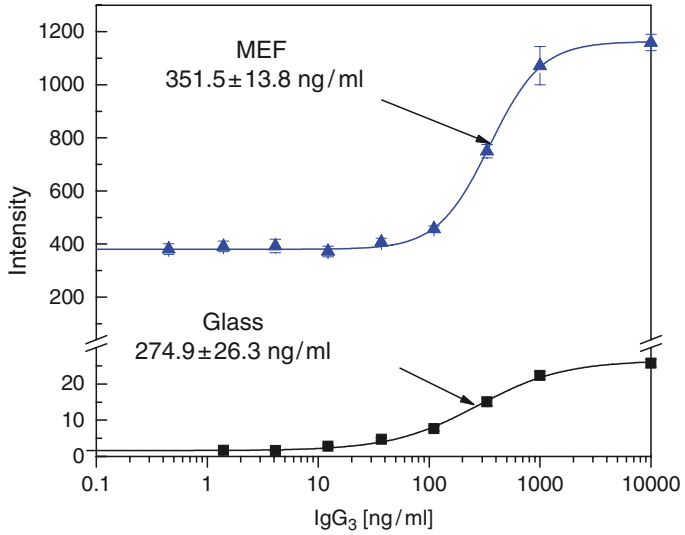

Fig. 13 Intensity-based Calibration Curves For IgG_3 immunoassays using glass and MEF substrates. The intensity readouts were performed in the presence of free probes (4 μg ml^{-1}) for the MEF substrate and after washing out for the glass

temperature. After incubation, the fluorescence intensity was measured in the presence of free probes on the MEF substrates. A control experiment was carried out on bare glass where unbound probes were washed out. The four-parameter logistic function was used which is recognized as the reference standard for fitting the mean concentration-response for immunoassays [52].

The clear advantage of the MEF-based assay is that there is no requirement for washing out unbound probes prior to readout and a substantial increase in the fluorescence signal. These two advantages led to a shortening of the procedures and to increased accuracy, which are important aspects in performing measurements as rapidly as possible with potential for real-time monitoring of bioprocess samples and binding interactions. Note that both calibration curves display a similar dynamic range for analyte concentration as can be judged by the midpoint values

of 351.5 ng ml^{-1} for MEF and 274.9 ng ml^{-1} for the glass surface, which were determined from the fit of data to the four-parameter logistic function that describes sigmoidal concentration-response relationships observed in immunoassays [52].

An additional improvement in sensitivity can be obtained when including the reduction in lifetime of the bound probes compared to the unbound probes. The interaction between fluorophores and surface plasmons of metallic particles causes the fluorescence lifetime to dramatically decrease compared to free fluorophores in solution. This difference is best manifested when using phase-modulation fluorometry. Phase-modulation (or frequency-domain) fluorometry is widely used in research and has proven to be a sensitive technique to detect the presence of low signals from short lifetime fluorophores in the presence of substantially larger signals from longer lifetime fluorophores [53].

In principle, for phase-modulation fluorometry, the excitation intensity light is sinusoidally modulated which results in modulated emission. Two parameters are measured, phase delay between excitation and emission intensity and modulation of fluorescence intensity. The relation between lifetime and measured phase shift (φ) and fluorescence modulation (m) for a single exponential intensity decay is given by the following equation,

$$\tan(\varphi) = \omega\tau, \tag{5}$$

$$m = \left[1 + (\omega\tau)^2\right]^{-\frac{1}{2}} \tag{6}$$

where ω, is the radial modulation frequency ($\omega = 2\pi f$, f is the modulation frequency in cycles per second) and τ, is the fluorescence lifetime. More complex equations describe the phase shift and modulation in the case of multi-exponential intensity decays [54].

Phase-modulation intensity decays of a Cy5-labeled reporter antibody when free in solution and when bound to the MEF substrate in the sandwich IgG_3 assay are shown in Fig. 14. The average lifetime of the free probe is reduced about fivefold when the probe binds to the analyte in the sandwich format. Because of the shorter lifetime of the bound probes, the value of the phase shifts are lower than for free probes (bottom curves in Fig. 14) and modulations are higher (two upper curves in Fig. 14). Consequently, this phase and modulation contrast between the free and bound probes, combined with the increased intensity from bound probes, creates a possibility for the design of a highly sensitive and accurate method for performing surface-based fluoroimmunoassays.

While accurate measurements of intensity decays require multi-frequency measurements of phase shifts and modulations, for sensing applications, measurements can be performed using a single modulation frequency. For example, using a frequency above 100 MHz one can see a large difference between values of phase and modulation for the Cy5-IgG probe when bound to the MEF substrate and free in solution. The phase shift calibration curves for the IgG_3 assay are shown in Fig. 15. The calibration curves were generated using two concentrations of the labeled antibody

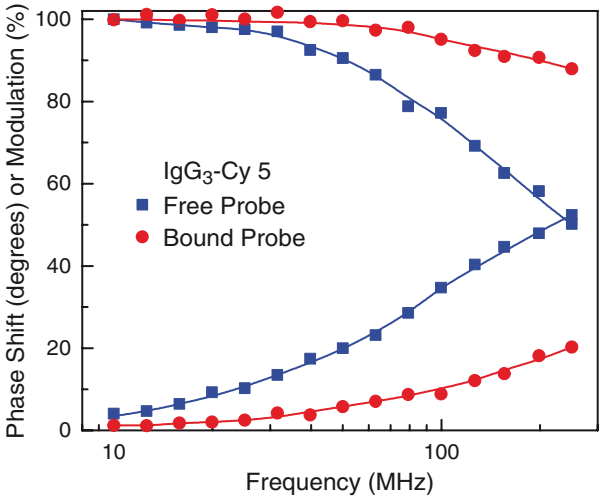

Fig. 14 Intensity decays of Cy5-labeled capture antibody when in buffer (*squares*) and when bound to MEF substrate. The excitation source was a RF-modulated red LED at 635 nm. The average lifetimes $<\tau> = \Sigma\alpha i\tau i$ [54] are 0.87 ns and 0.17 ns for free probe and bound probes, respectively

in solution (free probe), 4 μg ml^{-1} and 1 μg ml^{-1}. The differences in calibration curves are because of a different ratio of signal from bound to free probes. The ability to tune the detection sensitivity of the assay is a unique feature of the MEF-PM method. It is important to note that the phase shift calibration curve(s) are shifted towards lower antigen concentrations compared to the intensity measurements. For example, comparing the mid point value of 33.8 ng ml^{-1} for the phase shift (Fig. 15) to the value of 351.5 ng ml^{-1} for intensity (Fig. 13) results in a 10.3-fold sensitivity improvement. Additionally, the modulation data is complementary to the phase shift providing increased accuracy and further extension of the analytical range of the assay [51]. In fact, three parameters can be used together to determine the analyte concentration in biological samples (intensity, phase shift, and modulation) providing high accuracy and extended analytical range.

The MEF-PM approach was applied for detection of the concentration of monoclonal antibodies during the bioreaction process. Samples were collected 12, 42, and 72 h after the bioreaction process started. The samples were analyzed using measurements of the intensity, phase shift and modulation. Figure 16 shows the phase shift standard curve and fitted curves for selected cell culture samples, after 12 (1) and 72 h (6). The standard calibration curve was generated using a concentration of IgG_3 of 1 μg ml^{-1}, which was serially diluted in threefold increments with an additional 10 μg ml^{-1} of IgG_3 to obtain the saturation baseline.

The concentration of IgG_3 in the samples was determined from four dilutions of the original sample taken from the bioreaction chamber. The IgG_3 concentration values were determined from the shift of the mid point values relative to the standard calibration curve. Three parameters were used for calculation of the IgG_3

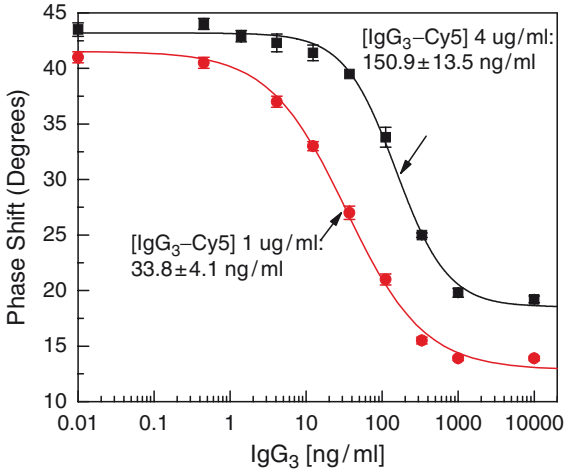

Fig. 15 Phase calibration curves for IgG3 immunoassay at two concentrations of free probes, 4 μg ml^{-1} and 1 μg ml^{-1}. The excitation was a red LED (635 nm) modulated at a frequency of 155 MHz

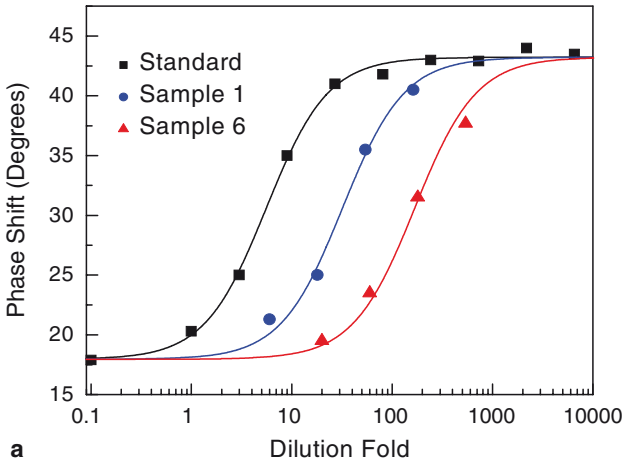

Fig. 16 Phase shift plots for standards and cell culture samples. The detection antibody concentration was 4 μg ml^{-1}

concentrations, phase shifts as shown in Fig. 16, modulations, and intensities (plots not shown). In parallel, concentrations of the IgG_3 were determined using an ELISA technique. Very good agreement between ELISA and MEF-PM values was found for the selected samples (Table 1). The average values for ELISA were determined from duplicate samples, while the average values for MEF-PM were determined from triplicate measurements of intensity, phase shift, and modulation as shown in Table 1 for each parameter measured. The larger variations of the

Table 1 Concentrations of IgG_3 in cell culture samples determined using the multiple analysis parameters of the MEF-PM method and ELISA

Sample #	1	3	6
ELISA	5.84 ± 0.28	12.60 ± 0.34	32.44 ± 2.14
Intensity	5.18 ± 0.73	9.55 ± 1.23	35.83 ± 4.28
Phase	5.97 ± 0.71	14.72 ± 1.53	30.77 ± 5.60
Modulation	5.58 ± 1.17	10.87 ± 0.53	33.45 ± 1.19

MEF-PM values compared to ELISA can be attributed to nonoptimized MEF substrates.

Further optimization in the preparation of MEF substrates, surface chemistry, and choice of fluorophore can be expected which will lead to enhanced sensitivity to about 100-fold compared to the conventional intensity-based assays. Additionally, low-cost LED-based phase-modulation instrumentation has already been demonstrated for similar measurements [55]. These advances open the door for compact benchtop or handheld instruments similar to those routinely used for glucose monitoring in a bioprocessing lab.

9 Surface Plasmon-Coupled Emission (SPCE)

In the previous sections we discussed the effects of metallic particles on fluorophores. We now consider the interactions of fluorophores with continuous metal films. Although the underlying electrodynamics mechanisms are the same for the interactions of fluorophores with metal particles or surfaces, the effects on fluorescence are very different. These differences arise from the defined geometry of a metal film and from the different nature of surface plasmons on sub-wavelength size particles and on planar surfaces. Surface plasmon-coupled emission (SPCE) is a phenomenon that occurs with excited fluorophores near continuous metallic surfaces covered with thin (~50 nm) metal films. These films are visually almost completely opaque. Excited fluorophores within about 100 nm of the surface result in strongly directional emission through the metal film and into the substrate. A large fraction of the total light energy is coupled into the substrate. This remarkable phenomenon is the result of near-field interactions of the excited fluorophores with the thin metal film, and is not simply a reflective or transmissive phenomenon. The SPCE emission is highly directional and appears at a well-defined angle. The emission spectrum is the same as that of the fluorophores, yet the emission is completely p-polarized.

A typical configuration for a SPCE experiment is shown in Fig. 17. We examined the fluorophore contained in a thin layer of polyvinyl alcohol (PVA) on a thin metal film. The sample was placed on a hemicylindrical prism and excited from the sample side of the prism (Fig. 17). In this case, the fluorophores are excited from the air side of the sample and the emission is observed on the distal glass side of

Fig. 17 Surface plasmon-coupled emission set up

the substrate. This is called the reverse Kretschmann (RK) configuration. Plasmons are not created on the metal surface by the light incident from this direction. For typical three-dimensional samples, not on a metal film, the emission is mostly the same in all directions (isotropic emission). In contrast, the fluorophores above the metal film yield a cone of emission into the substrate (Fig. 18). This means that almost all the emission into the substrate occurs at a defined angle θ_F relative to the normal axis. This result is even more remarkable when considering the optical properties of the metal films. These films are highly reflective and are visually almost opaque. SPCE is also observed with aluminum and gold (as shown in Fig. 18), which is surprising because both gold and aluminum are known to strongly quench fluorescence as discussed earlier.

Excited fluorophores in the near-field could create plasmons in the metal film, and these plasmons in turn radiate into the substrate [11–12]. Analytical theories have been developed for explaining SPCE [56–57]. An intuitive understanding of SPCE can be obtained from the principles of surface plasmon resonance (SPR) [58–63].

If SPCE displays the same characteristics as SPR, then fluorophores near the metal film will emit into the prism at angles defined by the emission wavelength and by the optical properties of the metal at the emission wavelength. We have observed the longer wavelength Stokes' shifted emission to occur at smaller angles. This separation of wavelength has been observed for fluorophores on silver films as shown in Fig. 19. This result shows that a simple metal film can be used to create directional emission and to separate different wavelengths. The wavelength dependence of SPR and SPCE results from the wavelength dependence of the optical constants of the metals.

Plasmon-coupled emission displays interesting polarization properties. SPR only occurs for the *p*-polarized component of the incident light because the projected wavevector of this component on the metal plane depends on the incident

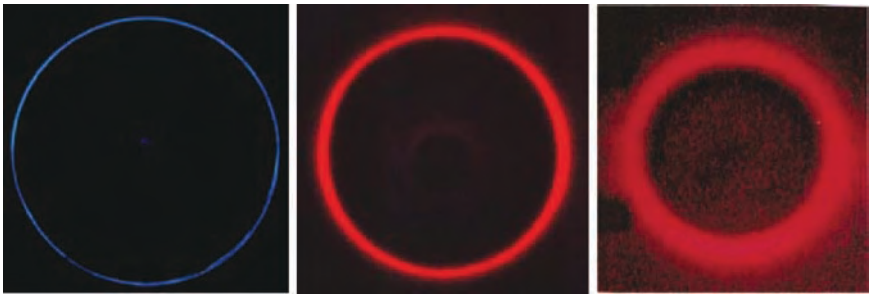

Fig. 18 Cone of emission for different fluorophores in PVA on aluminum (*left*), silver (*middle*), and gold (*right*) films

angle. Hence, SPCE is expected to be *p*-polarized at all angles around the cone, independently of the mode of excitation. The *p*-polarization of SPR and SPCE leads to the impression that only dipole measurements perpendicular to the metal surface will couple with the metal and cause SPCE. From the far-field the dipoles oriented perpendicular will result in *p*-polarized fields on the metal. However, the situation may be different for near-field interactions of the fluorophore with the metal surface, and we can expect to see coupling of fluorophores, parallel to the metal surface.

There are a number of publications on the theoretical aspects of fluorophores interacting with smooth metallic surfaces or mirrors [64–70]. This theory mostly describes fluorophores on or near thick metal films or mirrors. According to these papers there appears to be three possible processes for fluorophores near a smooth metal surface. The fluorophore can be quenched, can couple to surface plasmons or can emit into free-space. If the fluorophore is close to the surface ($d < 10$ nm) there is a high rate for radiationless deactivation and the emission appears to be quenched. At longer distances the reflected field interferes constructively or destructively, resulting in the oscillatory behavior reported for fluorophores in front of mirrors [68]. At distances from 20 to 100 nm the dominant decay rate is expected to be due to the surface plasmons. The coupling of fluorophores over these longer distances explains why gold films can also be used to couple emission into the prism. Forster transfer to the gold surface is likely to be minimal at distances above 10 nm where SPCE is still efficient. This is important for the applications of SPCE because coupling will occur over a significant volume in the sample allowing detection of lower overall analyte concentrations. In addition, larger depths for SPCE allows for construction of bioassays with multiple layers of proteins or the use of a separation layer to protect the metallic layer against corrosion and adverse chemical reactions.

During the past several years there have been an increased number of publications on SPCE to develop both a basic understanding of the phenomenon and to use SPCE for sensing applications [71–74]. Here we have chosen a few examples which illustrate the general features of SPCE and its applications. An important feature of SPCE is the distances over which the fluorophores can couple to surface

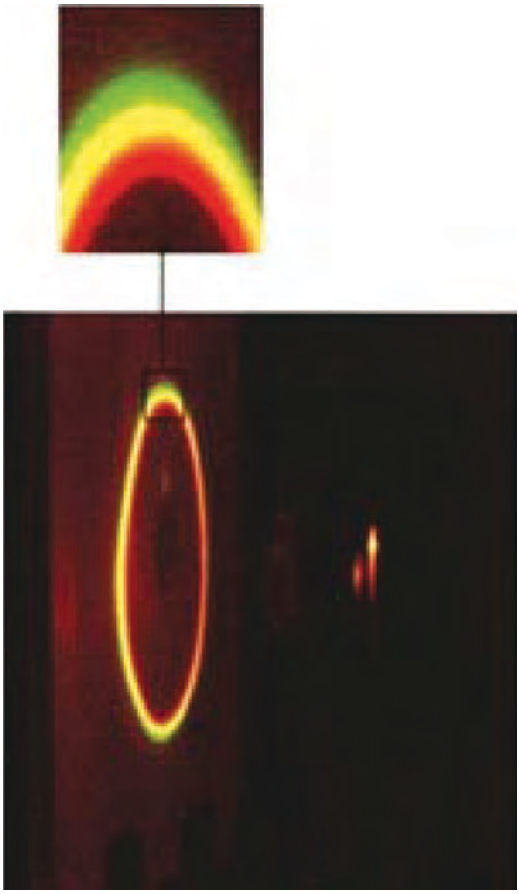

Fig. 19 Photograph of SPCE from the mixture of fluorophores using RK excitation and a hemispherical prism, with 532 nm excitation. Reprinted with permission from Elsevier Science [12]

plasmons. This distance dependence of SPCE can be studied by localizing fluorophores above the metal films using methods such as layer-by-layer assembly or Langmuir–Blodgett (LB) films [75–77]. Figure 20 shows the SPCE and free-space emission from a monolayer of a cyanine dye (DiI) at various distances over a 40-nm silver film. By free-space emission we mean the emission into the air above the metal film. As the fluorophores become more distant from the metal surface these couple with lower efficiency and there is an increase in the free-space intensity. The free-space emission decreases rapidly as the fluorophores move closer to the metal. As shown in Figs. 20 and 21, the free-space emission is very small below a distance of 20 nm, which is the distance for the highest SPCE intensity [77]. The angular SPCE distribution agrees well with the quantitative theoretical calculation of horizontally oriented transition dipole moment of DiI molecules relative to the metal surface as shown in Fig. 21. The differences in the intensities of radiation into the free space of the theoretical and experimental curves could result from the surface

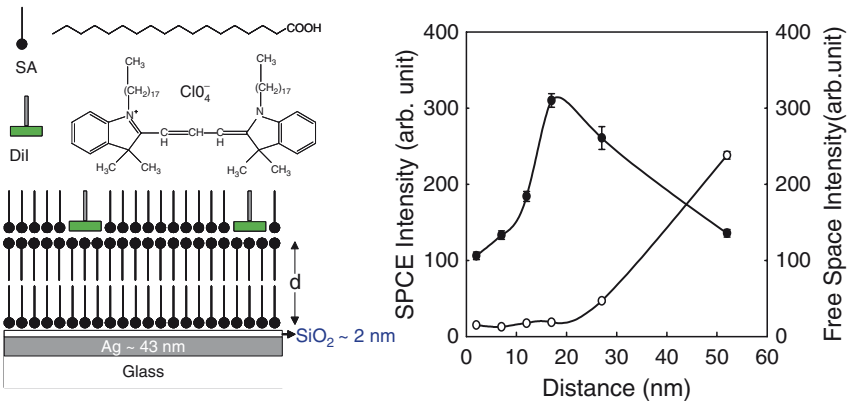

Fig. 20 (left panel) Schematic diagram of the sample including monolayers of stearic acid and the probe DiI. (right panel) SPCE and free space intensities of DiI-SA LB film as a function of distance from the silver surface

roughness of the metal substrate. However, it should be emphasized that the theoretical results presented here were calculated for the ideal case of perfectly planar substrates. A recent report [78] shows that colloidal silver nanoparticles self-assembled on top of continuous silver films can be used to increase the coupling efficiency of the excited state fluorophores to the surface plasmons in silver films, and thereby significantly enhance the SPCE signal.

The high efficiency of SPCE and the localized coupling efficiency suggest its use for bioassays. Because the coupling is optimal at a distance near 20 nm from the surface it is practical to design surface-bound assays. Figure 22 shows the emission spectra of an Alexa-labeled antibody bound to a capture antibody on a silver surface [79]. The Alexa emission can be detected even in whole blood with only a threefold decrease in intensity compared to the buffer control. The sensitivity of SPCE can be increased by the use of metal particles above the surface. Figure 23 shows various smooth metal surfaces with silver particles above the substrate. Silver particles above silver and gold films provide the highest intensities [80]. A unique feature of this result is that the emission intensities were measured from the sample side, not through the glass substrate. Normally we would refer to the sample side emission as free-space emission. However, the metal particles act as high k-vector sources which increase the coupling efficiency of light both into and out of the metal. The control of k-vectors near metal surfaces provides numerous opportunities for new types of devices for fluorescence sensing.

In the following paragraph, we describe waveguide effects in SPCE. These effects occur when the dielectric sample thickness above the metal film becomes comparable to the incident wavelength [81–82]. In this case, both *s* and *p*-polarized fields can exist in the dielectric. We examined SPCE for the probe Nile blue above a silver surface in polyvinyl alcohol films ranging in thickness from 44 to 595 nm. The SPCE ring for Nile blue with a thin dielectric film was similar to that shown in Fig. 18. For Nile blue in the 595-nm thick PVA film we observed multiple rings

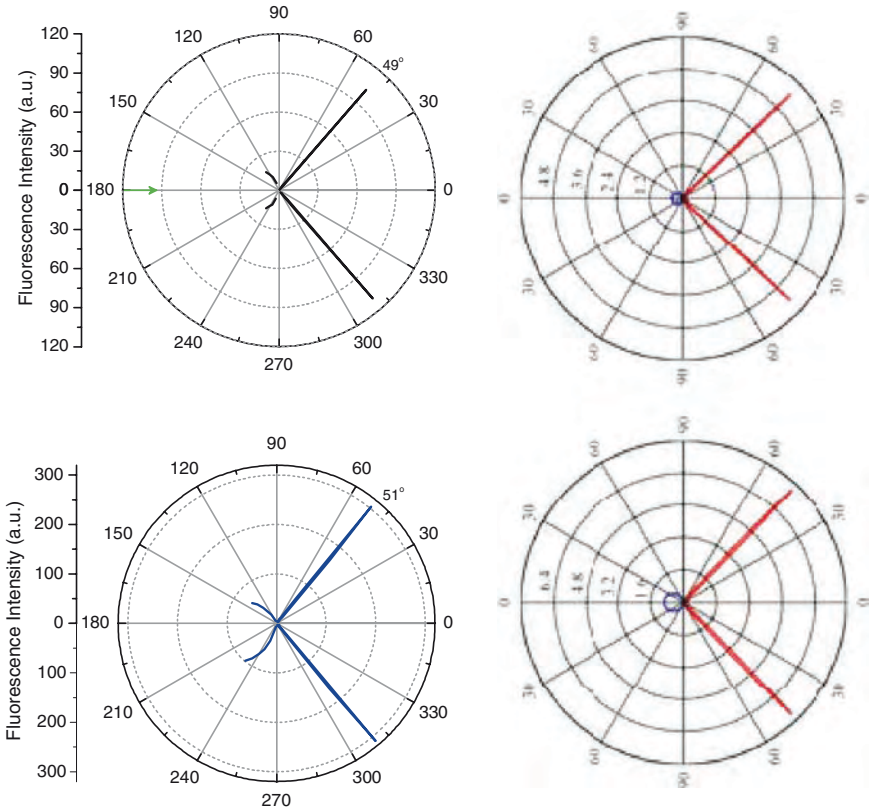

Fig. 21 Angle-dependent intensities (*left panel*) and calculated angular distributions (right panel) of radiation from a monolayer of DiI-SA at distances of 2 (*top*) and 17 (*bottom*) nm from the Ag surface

(Fig. 24). We examined the rings through a polarizer and found each ring to be partially extinguished depending on the orientation of the polarizer (Fig. 24). This effect is due to the alternate *s*- and *p*-polarization of the rings, which reflects the mode structure in the silver-PVA waveguide configuration. These results demonstrate that the single rings of SPCE represent only the simplest example of coupling fluorophores to metal surfaces. By controlling the dielectric thickness the SPCE angle and polarization can be controlled.

The high efficiency of coupling to metal films can be seen from the ability to image single molecules (Fig. 25). The single molecule intensities were found to be similar to those on glass alone, even though both the excitation and emission must pass across the silver film. In fact, other laboratories have reported increased single molecule intensities for probes above metal films [83–84]. In single molecule detection (vide infra), there is a direct comparison between the single molecule photon count rates. Hence, the single molecule measurements prove the high sensitivity of SPCE measurements.

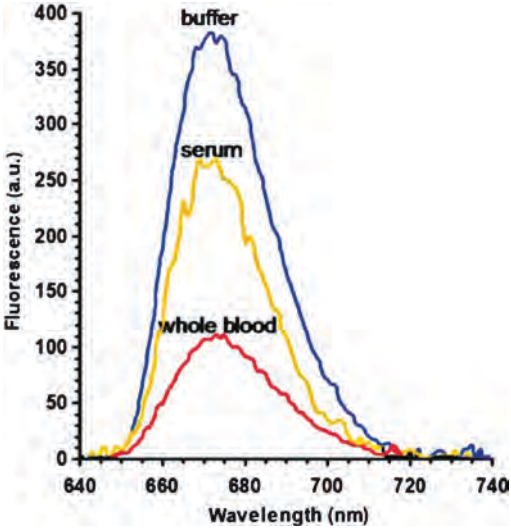

Fig. 22 Fluorescence spectra (SPCE) of the AlexaFluor 647-labeled anti-rabbit antibodies bound to the rabbit IgG immobilized on a 50-nm silver mirror surface observed in buffer, human serum, and human whole blood (Kretschmann (KR) configuration) [79]. Reprinted with permission from Elsevier Science

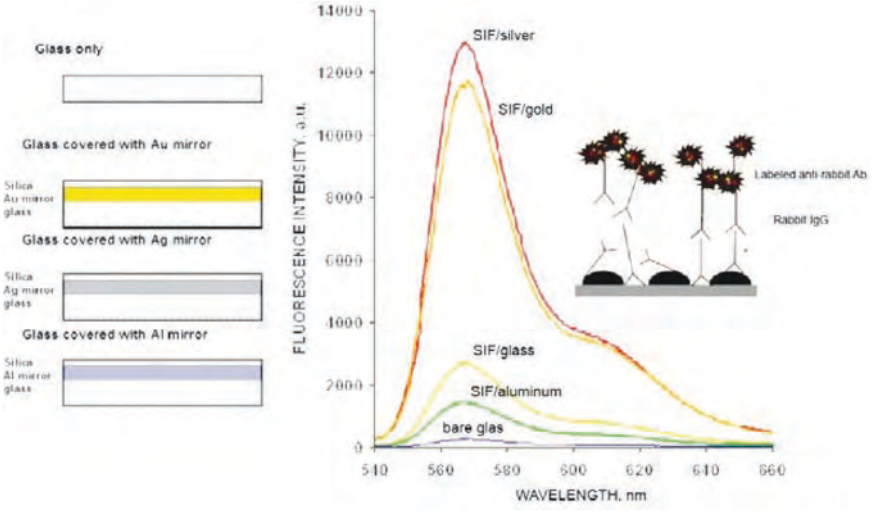

Fig. 23 *Left*: Schematic of substrates with silver particles above a smooth metal film. Each substrate has silver particles on the silica. *Right*: Emission spectra of AlexaFluor555-labeled IgG on the substrates. Revised from [80]. With permission from Elsevier Science

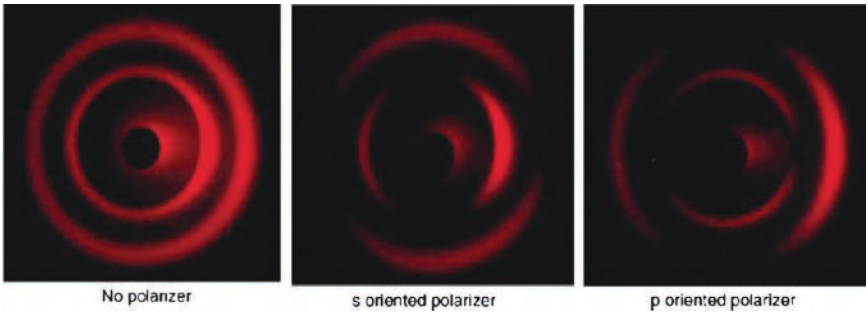

Fig. 24 Photograph of SPCE for 500-nm thick PVA film containing Nile blue. Revised from [81]. With permission from Elsevier Science

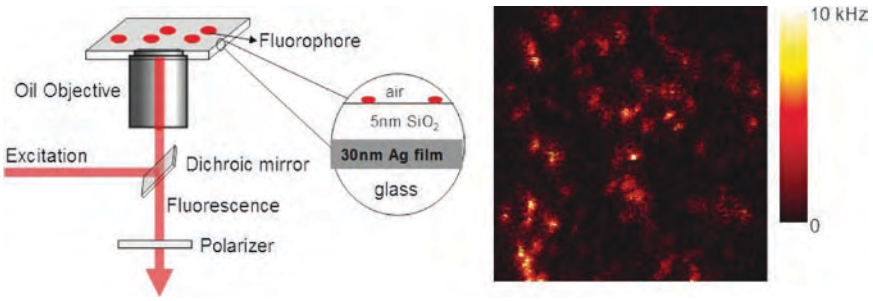

Fig. 25 Single molecule imaging of Cy5 through a silver film

10 Single Molecule Fluorescence near Metallic Nanostructures or Nanoparticles

There is a long history of using ensemble fluorescence spectroscopy to study fluorophores and fluorophore-labeled biomolecules. Even after these extensive experiments on ensembles the studies of single molecules have been informative. Single molecule detection (SMD) and fluorescence correlation spectroscopy (FCS) have been used to study a wide variety of biochemical phenomena such as protein folding and biomolecule association. Additional biochemical information is obtained because SMD and FCS measurements reveal the behavior of single molecules, rather than the ensemble average. For instance, SMD can be used to determine if a particular protein folds by a continuous or one-step mechanism. In previous sections, we have discussed a large number of ensemble experiments on fluorophore–metal interactions involving particulate metallic surfaces or smooth metal films that provided ensemble average data. These systems possess intrinsic heterogeneity because of the differences in particle size, distance to the surface and fluorophore orientation. A significant amount of

information can be obtained from single molecule or few-molecule spectroscopy (i.e., FCS) of fluorophores near metal particles. In some cases it may be preferable to resolve the underlying heterogeneity using SMD or FCS, rather than trying to prepare a chemically homogeneous sample.

SMD and FCS both reveal the properties of single molecules, but the experiments are rather different. With few exceptions, SMD is performed using single fluorophores or individually labeled biomolecules bound to a surface. This is necessary because single molecules can only be detected if the observed volume is small. FCS is used to measure freely diffusing molecules. Significant fluctuations in fluorescence intensity only occurs if the number of fluorophores observed at any given time are small, typically less than ten molecules. The observed volume is usually diffraction-limited. While the volume in FCS is limited to observe only a few molecules, there is another important reason for limiting the observed volume. The observation of single molecules is limited by the background emission and Raman scatter from the sample, both of which increase as the volume increases. Although not usually mentioned, the present instruments are nearly at the limits of sensitivity. Using typical optics and fluorophores, the theoretical maximum signal-to-noise (S/N) ratio for a single molecule is about 100-to-1, and most SMD measurements have a lower S/N ratio.

The brightness or emission rates determine the observability of a single molecule and the photostability determines the time that it can be observed prior to photobleaching. The observation times for single fluorophores are typically several seconds, after which irreversible photobleaching occurs. The ability to observe single molecules over the background is determined by the number of photons emitted per second. The number of detected photons per second is called the brightness. This is the reason SMD and FCS experiments are usually performed on fluorophores with high extinction coefficients, high quantum yields and short lifetimes. Such molecules have adequate brightness. A modest decrease in brightness makes a fluorophore not useful for single molecule studies.

The use of fluorophore–metal interactions has the potential to dramatically increase the detectability of single fluorophores for both SMD and FCS experiments. In the previous sections, we discussed ensemble MEF measurements that showed increased quantum yields, decreased lifetimes, and increased photostabilities. Decreased lifetimes will result in higher emission rates prior to saturation. This is possible because the fluorophores can cycle faster between the ground and excited states. Decreased lifetimes should result in higher photostability because there is less time for chemical reactions to occur in the excited state. Decreased lifetimes should also result in reduced blinking because there will be less time for the fluorophores to go to the triplet state. These effects will provide longer observation times prior to photobleaching. These effects could also be used for increased detectability of single molecules bound to surfaces that contain metallic structures, for either biophysical studies or high sensitivity assays.

Figure 26 shows scanning confocal images of single Cy5-labeled DNA molecules on a glass surface or on a SIF surface. When examined under the same conditions the Cy5-DNA molecules cannot be seen on glass but are easily observed on the SIF. In a

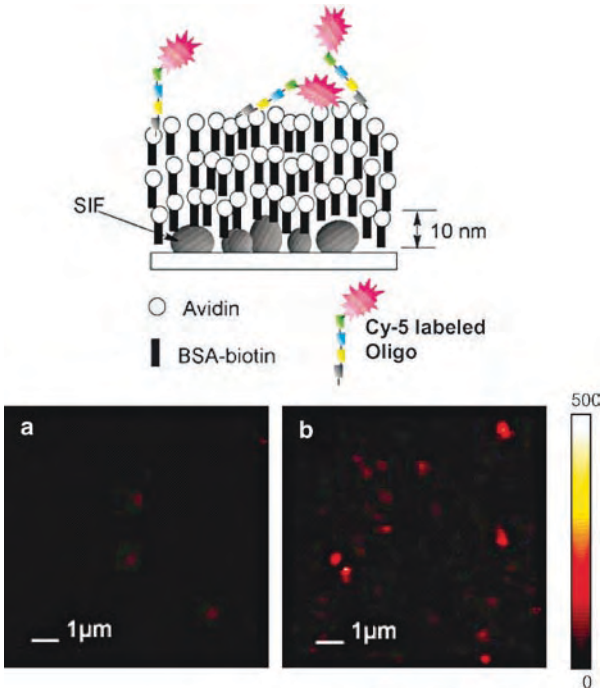

Fig. 26 Schematic of the sample. On SIF the Cy5-DNA is separated from the silver surface by a layer of BSA-biotin/avidin. Single molecule fluorescence images of Cy5-DNA on glass (*left*) and on a SIF (*right*). The laser intensities on the left (−700 nW) and right (−30 nW), the incident intensity is 23-fold less for the SIF. Revised and reprinted with permission from the American Chemical Society [86]

fluorescence image, a bright spot will be considered as the fluorescence emission from a single fluorophore if it meets several criteria: (a) the spot size is in the same order as the diffraction-limited size of the confocal set-up, (b) the signal level is consistent with the expected emission count rate from the single molecule, taking account of the quantum yield of the fluorophore, collection efficiency of the microscope and incident laser intensity, (c) the density of the spots are proportional to the concentration of the solution, (d) single-step photobleaching. Representative intensity-time traces of Cy5-labeled DNA molecules on a glass surface or on a SIF surface are shown in Fig. 27. The representative time traces show the higher intensity and increased photostability of Cy5-DNA near the silver particles. Intensity-time traces for a large number of Cy5-labeled DNA molecules on both surfaces were recorded and intensity histograms [85–86] were obtained as shown in Fig. 27. The intensity histograms show a large shift to higher intensities of the Cy5-labeled DNA molecules on the SIF compared to glass. In ensemble measurements we typically observed ten-fold enhancements on SIFs. However, the single molecule measurements showed that 35% of the molecules displayed more than 100-fold enhancement. This result suggests that it will be possible to synthesize fluorophore–metal complexes in which

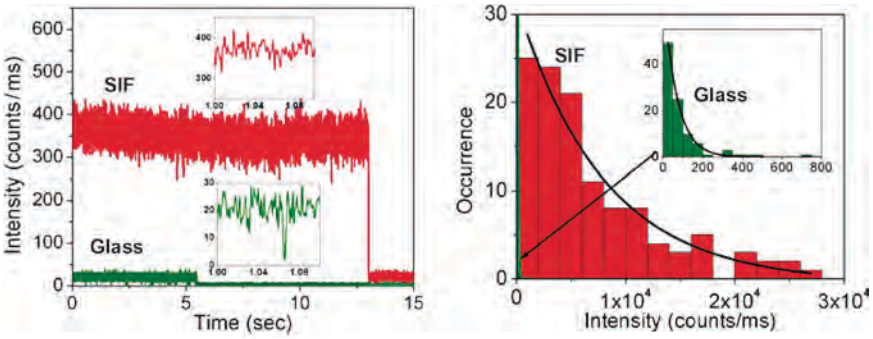

Fig. 27 Intensity-time traces (*left panel*) of Cy5-DNA on glass and SIF surfaces. Intensity histograms of Cy5-DNA on glass and SIFs (*right panel*). Revised and reprinted with permission from the American Chemical Society [86]

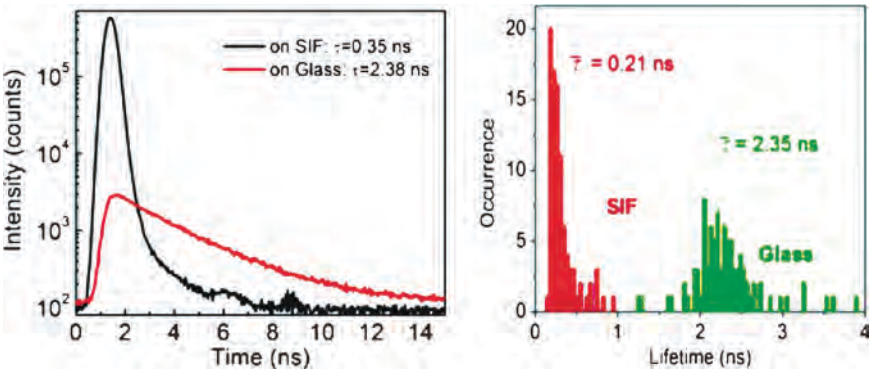

Fig. 28 Intensity decays and lifetime histograms of Cy5 on glass and SIF surfaces

all the fluorophores are enhanced more than 100-fold. In single molecule detection the most important spectral properties are the brightness and photostability. Cy5-labeled DNA molecules showed impressive photostability on SIF surfaces as shown in Fig. 27. The single molecule experiments are valuable because, by observation of many individual molecules, they suggest what is possible for favorable geometries.

The lifetimes of single Cy5 molecules were measured by time-correlated single-photon counting (TCSPC) and the lifetimes were recovered by nonlinear least-squares (NLLS). Figure 28 shows typical single molecule intensity decays on glass and SIFs. The lifetime of Cy5-DNA is dramatically shortened on the SIF. We measured the lifetimes of over 100 molecules, on either glass or silver, to determine the range of lifetimes present in each substrate. These histograms (Fig. 28) show that the lifetimes are at least tenfold shorter on the SIFs than on glass. The lifetime histogram on the SIF does not show any longer lifetime components comparable

to that on glass. This result is consistent with the binding of Cy5-SH-DNA directly to the silver particles and not to the glass between the particles.

Fluorescence emissions of organic fluorophores are generally intermittent (usually referred to as blinking) [87–89]. Thus, the continuous stream of emitted photons observed on long time scales is interrupted by so-called dark, or off, periods, i.e., a state that does not fluoresce. As a result, the single emitter is found to be intermittent: bright and dim/dark intervals randomly follow each other. Figure 29 presents the effects of nearby silver nanoparticles on the blinking of Cy5-DNA molecules. The Cy5 molecules on the glass surface clearly display fast emission intensity fluctuations with several long dark durations. However, when these Cy5 molecules are on the SIFs surface the blinking is very much suppressed as shown in the right panel of Fig. 29. The intensity time-traces also suggest enhanced photostability of fluorophores in the presence of silver nanostructures or nanoparticles.

In the previous section, we discussed the effects of silver nanostructures on the metal–fluorophore interactions. In the following section, we describe the effect of silver particle size on the photophysics of Cy5-DNA bound to spherical silver colloids ranging in diameter from 5 to 100 nm [90]. Suspension of silver colloids can be made with well-defined sizes and low heterogeneity. The silver particles were synthesized under controlled conditions with varied core sizes. These metal particles were succinimidylated via ligand exchange, bound by aminated oligonucleotide, and then hybridized by Cy5-labeled complementary single-stranded oligonucleotide. Size histograms of 5, 20, 50, 70, and 100 nm particles from the TEM images showed an average diameter equal to the target diameters. These particles displayed a switching of color from yellow to blue in water, corresponding to an increase of the size. The absorbance spectral measurements showed typical plasmon absorbances in the 400–550 nm region depending on the size of the silver particles, accompanied by simultaneous band broadenings (Fig. 30).

The intensity-time traces presented in Fig. 31 shows the overall trends of fluorophores when attached to metal particles of varied size. Most of the time traces showed clear one-step photobleaching, corresponding to typical behavior from a

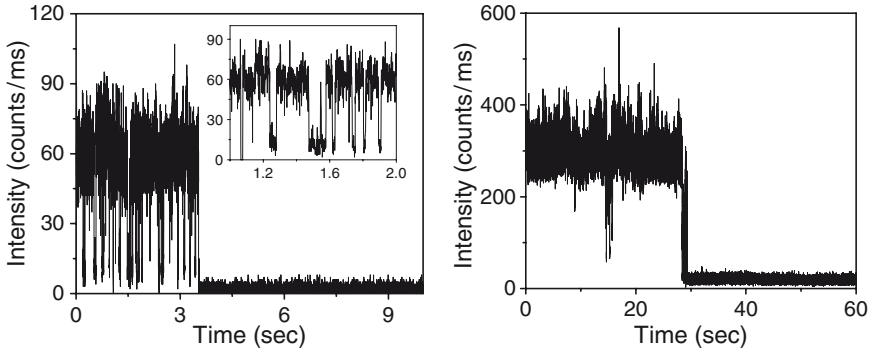

Fig. 29 Representative intensity-time traces of Cy5-DNA on glass (*left panel*) and SIF (*right panel*) surfaces. *Left panel* shows the usual blinking of Cy5 on glass

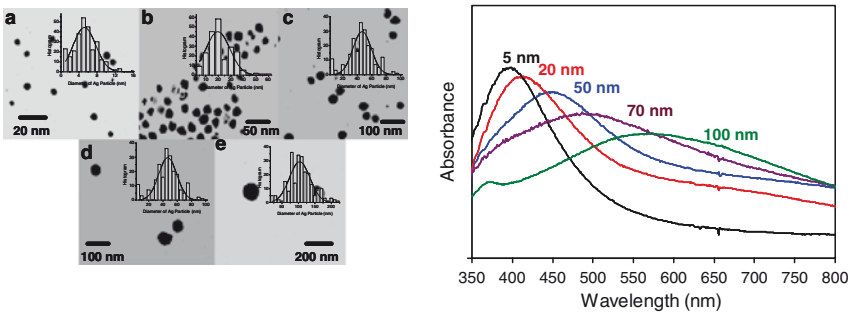

Fig. 30 Extinction spectra of silver colloids of various sizes and the TEM images of those particles. Revised and reprinted with permission from the American Chemical Society [90]

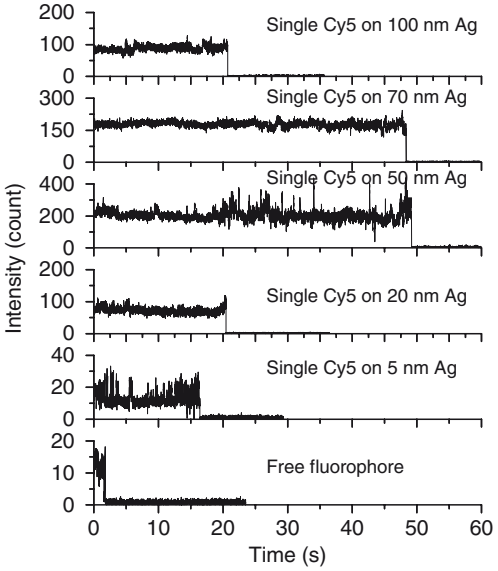

Fig. 31 Effects of silver particle size on single molecules of Cy5-DNA. A single Cy5-DNA molecule was attached to a silver particle by a surface reaction. Revised and reprinted with permission from the American Chemical Society [90]

single fluorophore. The single molecule intensity-time traces (as presented in Fig. 31) show that the intensity and photostability is strongly dependent on colloid size. Such data can be interpreted with analytical solutions of Maxwell's equations for such symmetrical systems [91–92]. However, it is useful to have an intuitive explanation of the effects. It seems logical that the 5 nm particle has no effect because smaller colloids may not display plasmons and/or the plasmon resonance wavelength is much shorter than the emission maxima (~670 nm) of Cy5. As the particle size increases the resonance shifts to longer wavelengths [90]. However, it seems that the overlap

is stronger with the 100 nm particle, not the 50 or 70 nm particle size which results in the brightest Cy5 emission. This lack of correspondence is probably due to the differences in the near-field and far-fields. The extinction spectra reflect the interaction of far-field light with the particle. The Cy5 intensities reflect the near-field interactions of the fluorophore with particles. These interactions may be optimal with the smaller particles because of the larger wave-vector (shorter effective wavelengths) in the near-field of the fluorophore.

We also noticed from the intensity-time traces (Fig. 31) that the fluorescence blinking was obviously reduced after binding the fluorophores on the metal particles. Hence, besides an increase of fluorescence intensity, the loading of fluorophore on the metal particle can also provide constant fluorescence signals without strong photoblinking. The intensity-time traces of Cy5 attached to a metal particle showed a significant extension of emissive (ON) time with the particle size (Fig. 31). Under the same conditions, free Cy5 in the absence of metal is bleached completely in 2 s but the single-labeled 50 and 70-nm silver particles are bleached in almost 50 s, 25-fold longer. The increase in photostability with the particle size is consistent with the trend of enhancement efficiency.

An alternative approach to achieve locally high fields is to use clusters of particles. It is well known that the local fields induced by incident light can become very large for closely spaced particles, in some cases up to a factor of 10^{13} [93–94]. We simulated the local fields induced between particle dimers included by the incident light (Fig. 32). The particles were assumed to be silver cylinders on a glass surface. The finite-differences time domain (FDTD) calculations show that for suitably spaced nanodots the field is almost completely localized in the gap between the particles (left, linear scale). Hence it is of interest to determine the effects of localizing a fluorophore between two colloids [95]. The silver particles with a 20 nm diameter

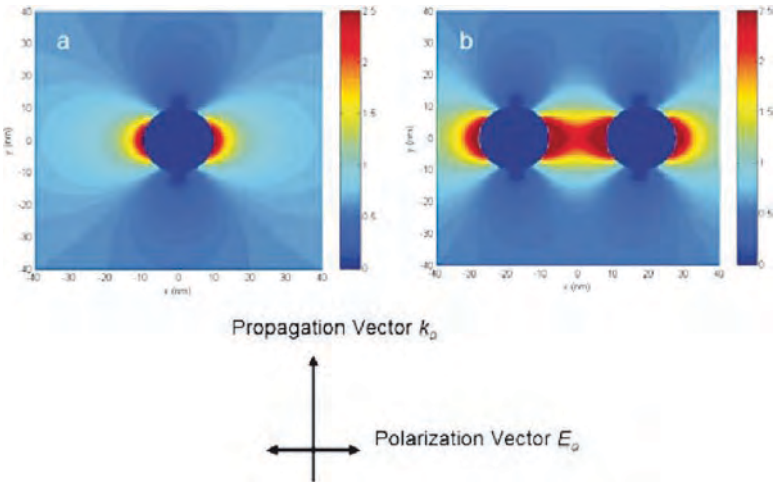

Fig. 32 Local fields induced by incident light from FDTD calculations. Reprinted with permission from the American Chemical Society [95]

were chemically bound with single-stranded oligonucleotides. The dimers were formed by hybridization with double-length single-stranded oligonucleotides that contained single Cy5 molecules. The time trace profile of the labeled metal dimers showed a higher intensity scale than the metal monomers, and the emission persisted much longer than the free fluorophores in the absence of metal particles (Fig. 33). This result suggests that biomolecule binding assays can be based upon clustering of metal particles near fluorophores.

Another opportunity using metal–fluorophore interactions is to increase the distances for energy transfer. FRET is arguably the most widely used fluorescence phenomenon, particularly in biotechnology and cell biology. FRET distances rarely exceed 6 nm. An increase in the FRET distances will be important in numerous applications of fluorescence, especially for determining the proximity of large biomolecular assembles and for FRET immunoassays for high molecular weight antigens. Since immunoassays are often performed in a sandwich format (Fig. 34) the distances between donors and acceptors are too large for useful amounts of FRET.

As a result FRET is infrequently used for sandwich immunoassays [96]. An increased distance for FRET will be useful in the study of large biomolecule complexes and in cell biology. For instance, suppose proteins on a cell membrane are too far apart for FRET (>10 nm) but still part of a macromolecular complex.

We have recently reported nearly twofold increases in the Forster distance (R_0), in both ensemble measurements and in single molecule measurements [97–98]. The single molecule experiments were performed using spherical colloidal silver nanoparticles. However, larger increases in FRET are expected for elongated particles as reported by the analytical solutions of Maxwell's equations for fluorophores (point dipoles) positioned near spherical and elongated silver colloids [99–101]. A value of the analytical solutions is an ability to understand the nature of the interactions.

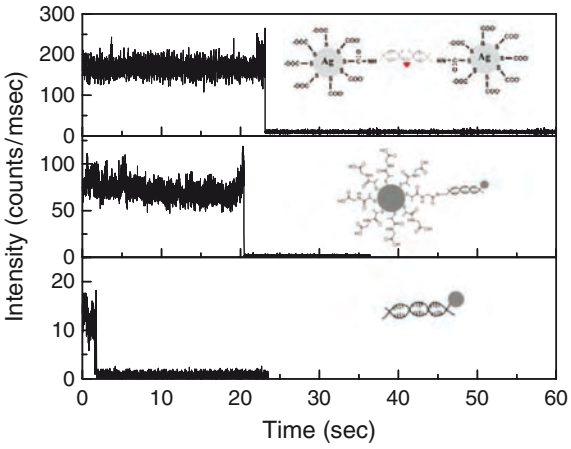

Fig. 33 Intensity traces and histograms for Cy5-DNA on a silver colloid dimer, bound to a single silver particle and without a silver particle. Revised and reprinted with permission from the American Chemical Society [95]

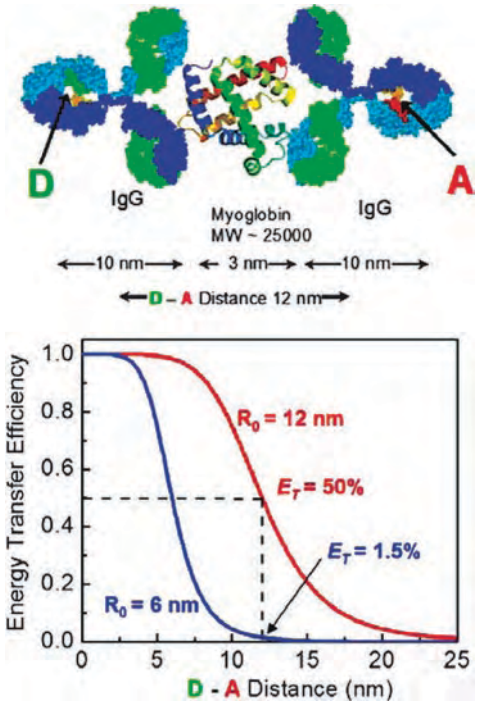

Fig. 34 Schematic of energy transfer in a sandwich assay with a change in R_0. For this D–A pair the transfer efficiency is close to 50% for the metal-enhanced R_0 = 12 nm and only 1.5% for R_0 = 6 nm without a metal particle

For instance, for metal-enhanced FRET, the effect was seen as a modification of the dipole–dipole interactions between the donor and acceptor. This interaction can result in increased or decreased rates of energy transfer, depending on the size and shape of the particles, the position and distance of the fluorophores from the surface, and the orientation of the dipoles relative to the metal surface. The importance of a larger effective Forster distance for immunoassays can be perceived from a specific example. For example, we use a sandwich assay with two IgG molecules and a relatively small antigen like the cardiac marker myoglobin with a molecular weight of 25,000 [102–104] as shown schematically in Fig. 33. If the donor D and acceptor A are located near the center of the IgG molecules they will be about 12 nm apart (Fig. 34). The value of typical Forster distances R_0 is rarely higher than 6 nm. As a result the transfer efficiency will be about 0.015, which is essentially undetectable. Now in the presence of a metal particle if the Forster distance could be increased by twofold, the transfer efficiency increases to 50% and is easily detectable. This example suggests that metal-enhanced FRET can be used to develop FRET immunoassays of large molecular weight antigens.

Single molecule FRET experiments can be used to determine the transfer efficiency of donor–acceptor pairs and the amount of FRET near metal particles [105–106]. We

have recently reported a systematic study on the effects of metal particle size, spacer distance between the donor and acceptor, and linker length of the donor–acceptor pair from the metal particle on metal-enhanced FRET. We prepared a donor and acceptor-labeled oligomer which contained a central amino group for binding to the colloid. The length of the oligomers was chosen so there was less than 10% transfer in the absence of the particle (Fig. 35). The transfer efficiency increased dramatically upon binding to the 15 nm colloid, and increased more with increasing particle size. The increase in transfer efficiency is consistent with a 1.7-fold increase in the Forster distance. Assuming the R_0 value in the absence of metal is 6 nm, the effective R_0 on the 80 nm particle is 10.2 nm, which is possibly one of the highest R_0 values which have been observed.

To date we have only investigated the effects of spherical particles on FRET. As mentioned earlier, the analytical theory suggests much higher rates of energy transfer when the donor—acceptor pairs are close to elongated particles [99–101]. Such long-range energy transfer may find uses in cell biology. It is known that cellular function can be affected by protein association in the external cell membrane, such as the receptors for epidermal growth factor (EGF). Suppose the EGF receptors are labeled with donors and acceptors, by using either labeled EGF or labeled antibodies to the receptor. Upon receptor association there will be minimal FRET because of the large size of the proteins. Now suppose one of the labeled proteins is bound to an ellipsoidal silver colloid about 100 nm long. Then it is possible that the colloid will facilitate FRET over this distance and detect receptor association. It may not be possible to measure the exact donor-to-acceptor distance using metal particles, but it may be possible to detect proximity over distances ranging from 10 to 100 nm. At present it is difficult to measure distances in this range. Electron microscopy requires fixed samples and the resolution of optical microscopy is limited to about 300 nm. Metal-enhanced FRET may allow measurement over this range of distances.

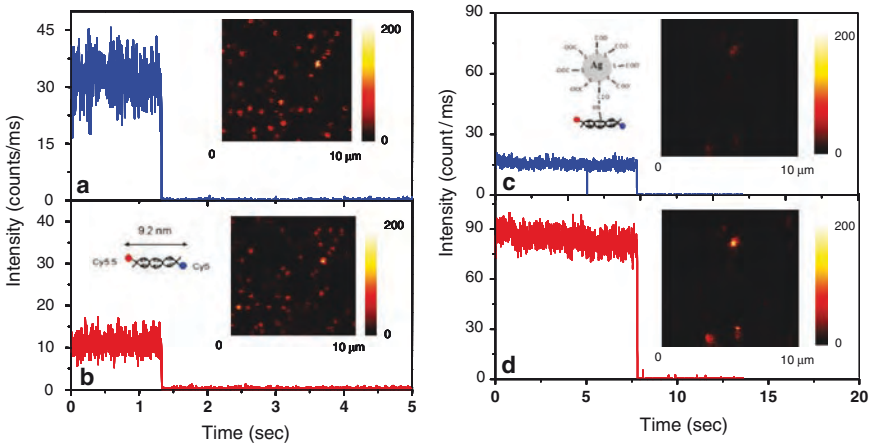

Fig. 35 Respective intensity-time trajectories of a free donor–acceptor pair as observed in the (**a**) donor channel or (**b**) the acceptor channel and a donor–acceptor pair bound to a silver particle (**c**) donor channel and (**d**) acceptor channel

11 Applications of Plasmon-Controlled Fluorescence

In the previous sections we described two types of metallic structures, metal particles for MEF and continuous thin metal films for SPCE. Metal particles and surfaces represent only a small fraction of the types of metallic structures which can be used to modify fluorescence. Many additional possibilities are available using metallic nanostructures with defined features. The underlying concept is to design the structure to provide wavevectors matching for the desired excitation and emission wavelengths. Perhaps the simplest example of such a structure is a metallic grating. By using a grating structure we can obtain the desired separation by controlling the dimensions of the grating.

The use of gratings for PCF can go beyond wavelength resolution. Metal gratings are being used to increase the light output of LEDs [107–108]. If the grating is two dimensional then the emission tends to beam away normal to the surface, with some angular separation of wavelengths. Additionally, gratings have been shown to be effective substrates for metal-enhanced fluorescence [109–110]. The enhancements depend on the wavelength of the fluorophore and the period of the grating. It seems likely that one and two-dimensional gratings will soon find use in surface-bound fluorescence assays. The sensitivities can be increased by a combination of MEF due to the patterned structure and by directing more of the emission towards the detector.

Novel devices for fluorescence can be designed using the unique transmission properties of nanohole arrays. One example is shown in Fig. 36 which consists of two nanohole arrays with different spacing between the nanoholes. One array can be designed to transmit shorter wavelength green light for excitation, and the second array can be designed to transmit the longer wavelength red emission. At present such a device may seem too expensive given the high cost of nanofabrication. However, there is rapid progress in high-throughput methods for nanofabrication. One example is micro-contact printing (MCP). This method depends on nanofabrication of a

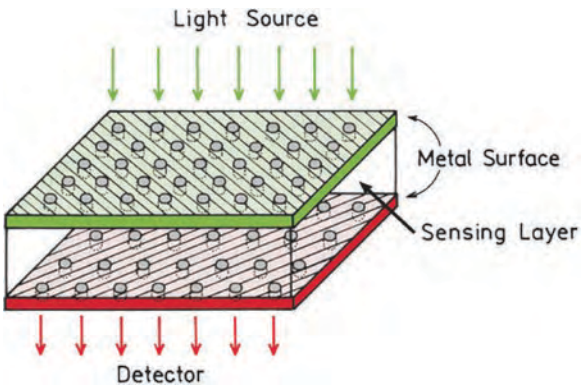

Fig. 36 Possible configuration for a sensor based on nanohole arrays

master structure [111–112]. This structure can then be used to fabricate elastomer replicas, typically in PDMS but other harder polymers can also be used. These replicate structures are then soaked in an ink such as a decanethiol and then used to print an image on a smooth metal film. The organic layer can protect the underlying metal from subsequent erosion steps, or be used to activate the printed regions by using a conjugatable thiol such as a decane thiol with a carboxyl group on the opposite end. By the use of MCP or some other high-throughput method metallic nanostructures can be made at very low cost.

It seems likely that elongated nanohole arrays will be used for fluorescence polarization immunoassays (FPI). These assays are widely used for monitoring of drugs and small molecule analytes [113]. A typical assay uses a labeled analyte analogue as a competitive ligand for the unlabeled analyte (Fig. 37). Suppose a capture antibody is bound to the metal surface and that a thin layer of sample is on top of the array. This sample will contain both bound and unbound labeled analyte. The polarization of this probe depends on whether it is free in solution or bound to the antibody. Suppose the sample is illuminated with light polarized along an axis of the nanoholes. The emission from the bound probe will be polarized and have a larger parallel component $I^{\parallel}$ along the excitation polarization. The emission from the unbound probe will be unpolarized with a larger component perpendicular ($I^{\perp}$) to the incident polarization. Since the transmission of the array depends on polarization, the intensities transmitted along each axis will reflect the relative contributions

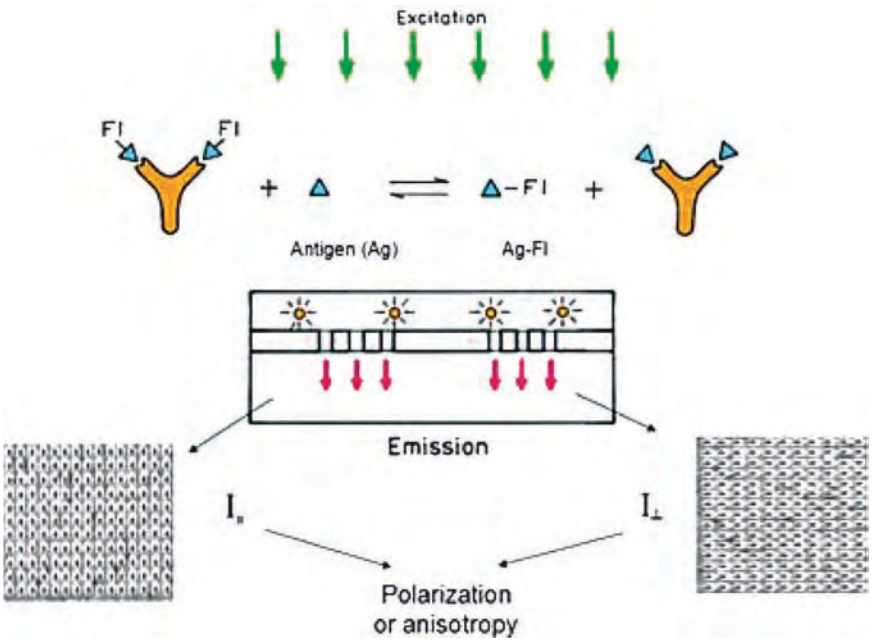

Fig. 37 Schematic of a thin-film-based fluorescence polarization assay

of the free and bound probes and the FPI instrument can consist of an elongated nanohole array. Careful design of the nanostructure geometry will be needed to obtain the needed selectivity to each polarized component of the emission [114–115].

12 Use of Metallic Nanostructures for Detection Beyond the Diffraction Limit

In classical far-field optics the spatial resolution is dictated by the spot size of the incident beam (i.e., about 300 nm across a diffraction limited spot) and about 2,000 nm along the optical axis, for a volume of about 1 fL. In order to observe single molecules their emission must be detectable above the Raman scatter and background emission from this volume. As a result single fluorophores can be observed only if these have high quantum yields and are contained in samples with low background emission. Conversely, if smaller volumes can be observed then it may become practical to detect single fluorophores with lower quantum yield fluorophores or detection of single molecules in samples like serum or blood with high background emission. Metallic nanostructures make it possible in some ways to reduce the observed volumes and with a spatial resolution that is well beyond the diffraction limit of the light [116]. One approach is to use the increased fields between pairs of particles. There are many published calculations of the fields between particle dimers [117–118]. However, these calculations do not directly reveal how these fields can be used to obtain sub-wavelength observation volumes. While the fields may be localized it is still necessary to illuminate the structure and the size of the incident beam is still limited by diffraction.

Figure 38 shows the simulated image of local fields induced between two nano-triangles due to the incident plane-wave illumination. The degree of localization is very strong for a pair of triangles. Interestingly, we calculated that even if the entire nanotriangle area were coated with fluorophores, about 25% of the emission would come from the 16 × 16-nm gap region occupying less than 1% of the area. The field calculation suggests that if the triangle pair is uniformly coated with fluorophores a large fraction of the total emission will come from those fluorophores between the tips of the triangle. These calculations suggest that particle clusters can be used to obtain reduced volumes with typical macroscopic optics used to illuminate particle clusters.

Another approach to obtain small volumes is to use the enhanced transmission through nanoholes. When nanoholes in metal films are illuminated there is typically an enhanced field in the nanohole or above the nanohole. This geometry may be preferred because the metal film is expected to block all the light so that the excitation field only exists in or above the nanohole. However, it is known that light incident on a single nanohole can induce plasmons on the distal side of the film [119] so that completely localized excitation may not always occur. Nonetheless, nanoholes are promising structures for obtaining small volumes.

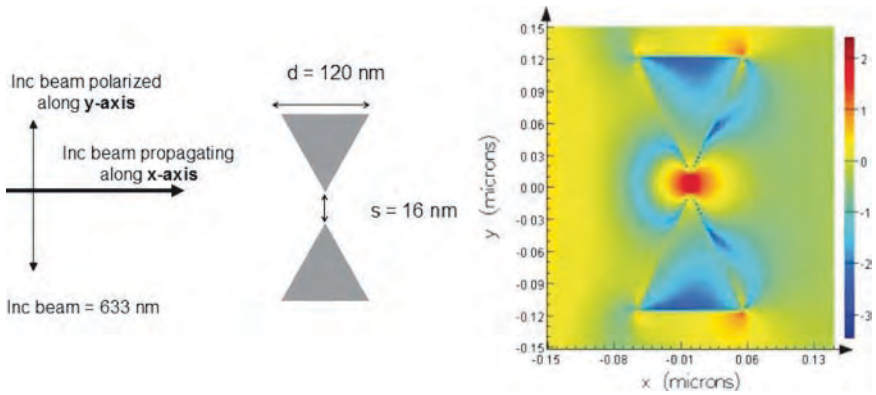

Fig. 38 FDTD calculations of the electric field due to plane-wave illuminations

Remarkably, the intensities from single molecules are enhanced several-fold compared to free solution [120–124].

There are several other methods being developed to obtain reduced volumes. One approach is to use sub-wavelength holes in an opaque film [125–126]. In this case only an evanescent wave can partially enter the nanohole and this evanescent wave serves as the excitation source. By SPCE the reduction in observation could be achieved and the advantage of SPCE is localization of the volume close to the metal surface rather than restraining the volume in three dimensions [127–128]. Microscopic application of surface plasmon-coupled emission also showed the reduction in observation volume down to 2 atto-liters [129]. A promising approach to obtain extremely small volume and optical field localized to about 5 nm is to employ tapered metallic waveguides [130].

13 Summary

In this review, the myriad forms of metal–fluorophore interactions are discussed and suggestions are made to show how these effects can create a new class of fluorescent probes, bioassays, and devices as well as novel experimental techniques. PCF provides unique opportunities for utilizing the effects of the near-fields created by the interaction of fluorophores with nearby plasmonic nanostructures, which results in fundamental changes in the fluorophore emission properties. Critical to the successful implementation of PCF lies in the ability to design effective nanostructures that can lead to high emission enhancements and high emission collection efficiency. Although the principles governing fluorophore–metal interactions are complex and involve both near- and far-field effects, PCF offers many interesting opportunities for the design of high-sensitivity bio-assays. A major advantage of using PCF is the ability to control

the excitation and emission processes of fluorescent molecules, and this complements existing technology that is used for designing and synthesizing new fluorescent probes. Additionally, PCF allows the spatial distribution of the emission to be controlled with nearby metallic nanostructures instead of the usual macroscopic optics.

Acknowledgments This work was supported by National Institutes of Health (Grant nos. HG002655, EB006521, and EB00682).

References

1. Strickler SJ, Berg RA (1962) Relationship between absorption intensity and fluorescence lifetimes of molecules. J Chem Phys 37:814–822
2. Yguerabide J, Yguerabide EE (1998) Light-scattering submicroscopic particles as highly fluorescent analogs and their use as tracer labels in clinical and biological applications: I. Theory. Anal Biochem 262:137–156
3. Yguerabide J, Yguerabide EE (1998) Light-scattering submicroscopic particles as highly fluorescent analogs and their use as tracer labels in clinical and biological applications: II. Experimental characterization. Anal Biochem 262:157–176
4. Schultz S, Smith SR, Mock JJ, Schulz DA (2000) Single target molecule detection with nonbleaching multicolor optical immunolabels. Proc Natl Acad Sci U S A 97:996–1001
5. Sokolov K, Follen M, Aaron J, Pavlova I, Malpica A, Lotan R, Richards-Kortum R (2003) Real-time vital optical imaging of precancer using anti-epidermal growth factor receptor antibodies conjugated to gold nanoparticles. Cancer Res 63:199–2004
6. Chowdhury MH, Gray SK, Pond J, Geddes CD, Aslan K, Lakowicz JR (2007) Computational study of fluorescence scattering by silver nanoparticles. J Opt Soc Am B 24:2259–2267
7. Mayergoyz ID, Zhang Z, Miano G (2007) Analysis of dynamics of excitation and dephasing of plasmon resonance modes in nanoparticles. Phys Rev Lett 98:147401–1/4
8. Pelton M, Liu M, Park S, Scherer NF, Guyor-Sionnest P (2006) Ultrafast resonant optical sensing from single gold nanorods: large nonlinearities and plasmon saturation. Phys Rev B 73:155419–1/6
9. Lakowicz JR (2001) Radiative decay engineering: biophysical and biomedical applications. Anal Biochem 298:1–24
10. Lakowicz JR, Shen Y, D'Auria S, Malicka J, Fang J, Gryczynski Z, Gryczynski I (2002) Radiative decay engineering. 2. Effects of silver island films on fluorescence intensity, lifetimes, and resonance energy transfer. Anal Biochem 301:261–277
11. Lakowicz JR (2004) Radiative decay engineering 3: surface plasmon coupled emission. Anal Biochem 324:153–169
12. Gryczynski I, Malicka J, Gryczynski Z, Lakowicz JR (2004) Radiative decay engineering 4: experimental studies of surface plasmon coupled emission. Anal Biochem 324:170–182
13. Sokolov K, Chumanov G, Cotton TM (1998) Enhancement of molecular fluorescence near the surface of colloidal metal films. Anal Chem 70:3898–3905
14. Amos RM, Barnes WL (1997) Modification of the spontaneous emission rate of Eu^{3+} ions close to a thin metal mirror. Phys Rev B 55(11):7249–7254
15. Barnes WL (1998) Fluorescence near interfaces: the role of photonic mode density. J Mod Opt 45(4):661–699
16. Weitz DA, Garoff S, Hanson CD, Gramila TJ (1982) Fluorescent lifetimes of molecules on silver-island films. Opt Lett 7(2):89–91
17. Aussenegg FR, Leitner A, Lippitsch ME, Reinisch H, Reigler M (1987) Novel aspects of fluorescence lifetime for molecules positioned close to metal surfaces. Surf Sci 139:935–945

18. Leitner A, Lippitsch ME, Draxler S, Riegler M, Aussenegg FR (1985) Fluorescence properties of dyes absorbed to silver islands, investigated by picosecond techniques. Appl Phys B 36:105–109
19. Sabanayagam C, Lakowicz JR (2007) Increasing the sensitivity of DNA microarrays by metal-enhanced fluorescence using surface-bound silver nanoparticles. Nucleic Acids Res 35:e13
20. Gu T, Whitesell JK, Fox MA (2003) Energy transfer from a surface bound arene to the gold core in fluorenyl-alkane-1-thiolate monolayer-protected gold clusters. Chem Mater 15:1358–1366
21. Gueroui Z, Liebchaber A (2004) Single-molecule measurements of gold quenched quantum dots. Phys Rev Lett 93:166108–166114
22. Ipe BI, Thomas KG (2002) Photoinduced charge separation in a fluorophore-Gold assembly. J Phys Chem B 106:18–21
23. Aguila A, Murray RW (2000) Monolayer-protected clusters with fluorescent dansyl ligands. Langmuir 16:5949–5954
24. Yun CS, Javier A, Jennings T, Fisher M, Hira S, Peterson S, Hopkins B, Reich NO, Strouse GF (2002) Nanometal surface energy transfer in optical rulers, breaking the FRET barrier. J Am Chem Soc 127:3115–3119
25. Fan C, Wang S, Hong JW, Bazan GC, Plaxco KW, Heeger AJ (2003) Beyond superquenching: hyper-efficient energy transfer from conjugated polymers to gold-nanoparticles. Proc Natl Acad Sci U S A 100:6297–6301
26. Zhang J, Lakowicz JR (2007) Metal-enhanced fluorescence of an organic fluorophore using gold particles. Opt Exp 15(5):2598–2606
27. Garoff S, Weitz DA, Alvarez MS, Gersten JI (1984) Electrodynamics at rough metal surfaces: photochemistry and luminescence of adsorbance near metal-island films. J Chem Phys 81(11):5189–5200
28. Ray K, Chowdhury M, Lakowicz JR (2007) Aluminum nano-structured film as a substrate for enhanced fluorescence in the ultraviolet – blue spectral region. Anal Chem 79:6480–6487
29. Ray K, Badugu R, Lakowicz JR (2006) Metal-enhanced fluorescence from CdTe nanocrystals: a single-molecule fluorescence study. J Am Chem Soc 128:8998–8999
30. Okamoto K, Vyawahare S, Scherer A (2006) Surface-plasmon enhanced bright emission from CdSe quantum-dot nanocrystals. J Opt Soc Am B 23:1674–1678
31. Shimizu KT, Woo WK, Fisher BR, Eisler HJ, Bawendi MG (2002) Surface-enhanced emission from single semiconductor nanocrystals. Phys Rev Lett 89:117401–1/4
32. Chowdhury MH, Ray K, Aslan K, Lakowicz JR, Geddes CD (2007) Enhanced fluorescence of phycobiliproteins from plasmonic nanostructures. J Phys Chem C 111:18856–18863
33. Lakowicz JR, Maliwal BP, Malicka J, Gryczynski Z, Gryzynski I (2002) Effects of silver island films on the luminescent intensity and decay times of lanthanide chelates. J Fluoresc 12(3/4):431–437
34. Wu M, Lakowicz JR, Geddes CD (2005) Enhanced lanthanide luminescence using silver nanostructures: opportunities for a new class of probes with exceptional spectra characteristics. J Fluoresc 15:53–59
35. Daniel E, Weber G (1966) Cooperative effects in binding by bovine serum albumin, I: the binding of 1-anilino-8-naphthalenesulfonate. Fluorimetric titrations. Coop Effects Binding Albumin 5:1893–1900
36. Slavik J (1982) Anilinonaphthalene sulfonate as a probe of membrane composition and function. Biochim Biophys Acta 694:1–25
37. Benson SC, Zeng Z, Glazer AN (1995) Fluorescence energy-transfer cyanine heterodimers with high affinity for double-stranded DNA. Anal Biochem 231:247–255
38. Haq I, Ladbury JE, Chowdhry BZ, Jenkins TC, Chaires JB (1997) Specific binding of Hoechst 33258 to the D(CGCAAATTTGCG)$_2$ duplex: calorimetric and spectroscopic studies. J Mol Biol 271:244–257
39. Glazer AN, Peck K, Matheis RA (1990) A stable double-stranded DNA ethidium homodimer complex: application to picogram fluorescence detection of DNA in agarose gels. Proc Natl Acad Sci U S A 87:3851–3855

40. Rye HS, Yue S, Wemmer DE, Quesada MA, Haugland RP, Mathies RA, Glazer AN (1992) Stable fluorescent complexes of double-stranded DNA with bis-intercalating asymmetric cyanine dyes: properties and applications. Nucleic Acids Res 20(11:):2803–2812
41. Malicka J, Gryczynski I, Lakowicz JR (2003) DNA hybridization assays using metal-enhanced fluorescence. Biochem Biophys Res Commun 306:213–218
42. Enderlein J (2002) Spectral properties of a fluorescing molecule within a spherical metallic cavity. Phys Chem Chem Phys 4:2780–2786
43. Enderlien J (2002) Theoretical study of single molecule fluorescence in a metallic nanocavity. Appl Phys Lett 80:315–317
44. Zhang J, Gryczynski I, Gryczynski Z, Lakowicz JR (2006) Dye-labeled silver nanoshell – bright particle. J Phys Chem B 110:8986–8991
45. Aslan K, Lakowicz JR, Geddes CG (2007) Metal enhanced fluorescence solution-based sensing platform 2: fluorescent core-shell Ag@SiO_2 nanoballs. J Fluoresc 17:127–131
46. Aslan K, Wu M, Lakowicz JR, Geddes CG (2007) Fluorescent core – shell Ag@SiO_2 nanocomposites for meta-enhanced fluorescence and single nanoparticle sensing platforms. J Am Chem Soc 129:1524–1425
47. Hemmila IA (1991) Applications of fluorescence in immunoassays. John Wiley & Sons, New York, 360 p
48. Soini E, Hemmila IA, Dahlen D (1995) Time-resolved fluorescence in biospecific assays (review). Pharmacol Ther 66:207–235
49. Yan Y, Marriott G (2003) Analysis of protein interactions using fluorescence technologies. Curr Opin Chem Biol 7:635–640
50. Goldsby RA, Kindt TJ, Osborne BA, Kuby J (2003) Enzyme-linked immunosorbent assay. In: Immunology, 5th edn. Freeman, New York, pp. 148–160
51. Szmacinski H, Smith D, Hanson MA, Kostov Y, Lakowicz JR, Rao G (2008) A novel method for monitoring monoclonal antibody production during cell culture. Biotechnol Bioengin 100:448–457
52. Findlay JWA, Smith WC, Lee JW, Nordblom GD, Das I, DeSilva BS, Khan MN, Bowsher RR (2000) Validation of immunoassays for bioanalysis: a pharmaceutical industry perspective. J Pharm Biomed Anal 21:1249–1273
53. Szmacinski H, Lakowicz JR (1999) Measurement of the intensity of long lifetime luminophores in the presence of background signals using phase-modulation fluorometry. Appl Spectrosc 53:1490–1494
54. Lakowicz JR (2006) Principles of fluorescence spectroscopy, 3rd edn. Springer Science, New York, pp. 158–204
55. Harms P, Sipior J, Ram N, Carter GM, Rao G (1999) Low cost phase-modulation measurements of nanosecond fluorescence lifetimes using a lock-in amplifier. Rev Sci Instrum 70(2):1535–1539
56. Calander N (2005) Surface plasmon-coupled emission and Fabry-Perot resonance in the sample layer: a theoretical approach. J Phys Chem B 109:13957–13956
57. Calander N (2004) Theory and simulation of surface plasmon-coupled directional emission from fluorophores at planar structures. Anal Chem 76:2168–2173
58. Salamon Z, Macleod HA, Tollin G (1997) Surface plasmon resonance spectroscopy as a tool for investigating the biochemical and biophysical properties of membrane protein systems. I: Theoretical principles. Biochim Biophy Acta 1331:117–129
59. Melendez J, Carr R, Bartholomew DU, Kukanskis K, Elkind J, Yee S, Furlong C, Woodbury R (1996) A commercial solution for surface plasmon sensing. Sens Actuators B 35–36:212–216
60. Liedberg B, Lundstrom I (1993) Principles of biosensing with an extended coupling matrix and surface plasmon resonance. Sens Actuators B 11:63–72
61. Cooper MA (2002) Optical biosensors in drug discovery. Nat Rev 1:515–528
62. Wegner GJ, Lee HJ, Corn RM (2002) Characterization and optimization of peptide arrays for the study of epitope-antibody interactions using surface plasmon resonance imaging. Anal Chem 74:5161–5168

63. Natan MJ, Lyon LA (2002) Surface plasmon resonance biosensing with colloidal Au amplification. In: Feldheim DL, Foss CA (eds.) Metal nanoparticles: synthesis, characterization, and applications. Marcel Dekker, New York, pp. 183–205
64. Raether H (1977) Surface plasmon oscillations and their applications. Physics of thin films. In: Hass G, Francombe MH, Hoffman RW (eds.) Advances in research and development. Academic Press, New York, Vol. 9, pp. 145–261
65. Yih J, Chien F, Lin C, Yau H, Chen S (2005) Angular interrogation attenuated total reflection metrology system for plasmonic structures. Appl Opt 44:6155–6162
66. Skivesen N, Horvath R, Pederson HC (2005) Optimization of metal-clad waveguide sensors. Sens Actua B 106:668–676
67. Barnes WL (1998) Fluorescence near interfaces: the role of photonic mode density. J Mod Opt 45(4):661–699
68. Drexhage KH (1970) Influence of a dielectric interface on fluorescence decay time. J Luminescence 2:693–701
69. Benner RE, Dornhaus R, Chang RK (1979) Angular emission profiles of dye molecules excited by surface plasmon waves at a metal surface. Opt Commun 30(2):145–149
70. Weber WH, Eagen CF (1979) Energy transfer from an excited dye molecule to the surface plasmons of an adjacent metal. Opt Lett 4(8):236–238
71. Isfort G, Schierbaum K, Zerulla D (2006) Causality of surface plasmon polariton emission processes. Phys Rev B 73:033408–1/4
72. Chowdhury MH, Malyn SN, Aslan K, Lakowicz JR, Geddes JR (2006) Multicolor directional surface plasmon coupled chemiluminescence. J Phys Chem B 110:22644–22651
73. Kostov Y, Smith DS, Tolosa L, Rao G, Gryczynski I, Gryczynski Z, Malicka J, Lakowicz JR (2005) Directional surface plasmon-coupled emission from a 3 nm green fluorescent protein monolayer. Biotechnol Prog 21:1731–1735
74. Neal TD, Okamoto K, Scherer A (2005) Surface plasmon enhanced emission from dye doped polymer layers. Opt Exp 13(14):5522–5527
75. Ray K, Badugu R, Lakowicz JR (2007) Sulforhodamine adsorbed Langmuir–Blodgett layers on silver island films: effect of probe distance on the metal-enhanced fluorescence. J Phys Chem C 111:7091–7097
76. Ray K, Badugu R, Lakowicz JR (2007) Polyelectrolyte layer-by-layer assembly to control the distance between fluorophores and plasmonic nanostructures. Chem Mater 111:7091–7097
77. Ray K, Szmacinski H, Enderlein J, Lakowicz JR (2007) Distance dependence of surface plasmon-coupled emission observed using Langmuir—Blodgett films. Appl Phys Lett 90:251116–1/3
78. Chowdhury MH, Ray K, Geddes CD Lakowicz JR (2008) Use of silver nanoparticles to enhance surface plasmon-coupled emission (SPCE). Chem Phys Lett 452:162–167
79. Matveeva EG, Gryczynski Z, Malicka J, Lukomska J, Makowiec S, Berndt KW, Lakowicz JR, Gryczynski I (2005) Directional surface plasmon-coupled emission: application for an immunoassay in whole blood. Anal Biochem 344:161–167
80. Matveeva EG, Gryczynski I, Barnett A, Leonenko Z, Lakowicz JR, Gryczynski Z (2007) Metal particle-enhanced fluorescent immunoassays on metal mirrors. Anal Biochem 363:239–245
81. Gryczynski I, Malicka J, Nowaczky K., Gryczynski Z, Lakowicz JR (2006) Waveguide-modulated surface plasmon-coupled emission of Nile blue in poly(vinyl alcohol) thin films. Thin Solid Films 510:15–20
82. Gryczynski I, Malicka J, Nowaczyk K, Gryczynski Z, Lakowicz JR (2004) Effects of sample thickness on the optical properties of surface plasmon-coupled emission. J Phys Chem B 108:12073–12083
83. Stefani FD, Vasilev K, Bocchio N, Stoyanova N, Kreiter M (2005) Surface-plasmon-mediated single molecule fluorescence through a thin metallic film. Phys Rev Lett 94:023005–1/4
84. Vasilev K, Knoll W, Kreiter M (2004) Fluorescence intensities of chromophores in front of a thin metal film. J Chem Phys 120(7):3439–3445

85. Fu Y, Lakowicz JR (2006) Enhanced fluorescence of Cy5-labeled DNA tethered to silver island films: fluorescence images and time-resolved studies using single-molecule spectroscopy. Anal Chem 78:6238–6245
86. Fu Y, Lakowicz JR (2006) Enhanced fluorescence of Cy5-labeled oligonucleotides near silver island films: a distance effect study using single molecule spectroscopy. J Phys Chem B 110:22557–22562
87. Moerner WE (1997) Those blinking single molecules. Science 277:1059–1060
88. Dickson R, Cubitt A, Tsien R, Moerner WE (1997) On/off blinking and switching behaviour of single molecules of green fluorescent protein. Nature 388:355–358
89. Rasnik I, McKinney SA, Ha T (2006) Nonblinking and long lasting single molecule fluorescence imaging. Nat Methods 3:891–893
90. Zhang J, Fu Y, Chowdhury MH, Lakowicz JR (2008) Single molecule studies on fluorescently labeled particles: effects of particle size. J Phys Chem C 112:18–26
91. Ford GW, Weber WH (1984) Electromagnetic interactions of molecules with metal surfaces. Phys Rep 113(4):195–287
92. Gersten J, Nitzan A (1981) Spectroscopic properties of molecules interacting with small dielectric particles. J Chem Phys 75(3):1139–1152
93. Kneipp K, Kneipp H, Deinum G, Itzkan I, Dasari RR, Feld MS (1998) Single-molecule detection of a cyanine dye in silver colloidal solution using near-infrared surface-enhanced Raman scattering. Appl Spectrosc 52(2):175–178
94. Kneipp K, Wang Y, Kneipp H, Perelman L, Itzkan I, Dasari RR, Feld MS (1997) Single molecule detection using surface-enhanced Raman scattering (SERS). Phys Rev Lett 78(9):1667–1670
95. Zhang J, Fu Y, Chowdhury MH, Lakowicz JR (2007) Metal-enhanced single-molecule fluorescence on silver particle monomer and dimer: coupling effect between metal particles. Nano Lett 7:2101–2107
96. Ullman EF, Schwarzberg M, Rubenstein KE (1976) Fluorescent excitation transfer immunoassay: a general method for determination of antigens. J Biol Chem 251(14):4172–4178
97. Malicka J, Gryczynski I, Kusba J, Lakowicz JR (2003) Effects of metallic silver island films on resonance energy transfer between N,N′-(dipropyl)-tetramethyl-indocarbocyanine (Cy3)- and N,N′(dipropyl)-tetramethyl-indodicarbocyanine (cy5)-labeled DNA. Biopolymers 70:595–603
98. Zhang J, Fu Y, Lakowicz JR (2007) Enhanced Forster resonance energy transfer (FRET) on a single metal particle. J Phys Chem C 111:50–56
99. Gersten JI, Nitzan A (1983) Accelerated energy transfer between molecules near a solid particle. Chem Phys Lett 104:31–37
100. Hua XM, Gersten JI, Nitzan A (1985) Theory of energy transfer between molecules near solid state particles. J Chem Phys 83:3650–3654
101. Gersten JI (2005) Theory of fluorophore-metallic surface interactions. In: Topics in fluorescence spectroscopy. Radiative decay engineering, Vol. 8. Springer, New York, p. 197
102. Christenson RH, Azzazy HME (1999) Evidence based approach to practice guides and decision thresholds for cardiac markers. Scand J Clin Lab Invest 59(Suppl 230):90–102
103. Newby LK, Storrow AB, Gibler WB, et al. (2001) Bedside multimarker testing for risk stratification in chest pain units: the chest pain evaluation by creatine kinase-MB, myoglobin, and troponin I(CHECKMATE) study. Circulation 103:1832–1837
104. Christenson RH, Azzazy HME (1998) Biochemical markers of the acute coronary syndromes. Clin Chem 44:1855–1864
105. Zhang Z, Fu Y, Lakowicz JR (2007) Enhanced Forster resonance energy transfer (FRET) on a single metal particle. J Phys Chem C 111:50–56
106. Zhang Z, Fu Y, Lakowicz JR (2007) Enhanced Forster resonance energy transfer (FRET) on single metal particle 2: dependence on donor-acceptor separation distance, particle size, and distance from metal surface. J Phys Chem C 111:11784–11792
107. Gifford DK, Hall DG (2002) Emission through one of two metal electrodes of an organic light-emitting diode via surface-plasmon cross coupling. Appl Phys Lett 81(23):4315–4317

108. Feng J, Okamoto T, Kawata S (2005) Highly directional emission via coupled surface-plasmon tunneling from electroluminescence in organic light-emitting devices. Appl Phys Lett 87:241109–1/3
109. Matthews DR, Summers HD, Njoh k, Chappell S, Errington R, Smith P, Pope I, Barber P, Vojnovic B, Ameer-Beg S (2007) A fluorescence biochip with a plasmon active surface. Proc SPIE 6450:645006–1/8
110. Hung Y-J, Smolyaninov II, Davis CC (2006) Fluorescence enhancement by surface gratings. Opt Exp 14(22):10825–10830
111. Xia Y, Whitesides GM (1998) Soft lithography. Annu Rev Mater Sci 28:153
112. Milan M, Whitesides GM (1995) Patterning self-assembled monolayers using microcontact printing: a new technology for biosensors. TIBTECH 13:228–231
113. Dandliker WB, de Saussure VA (1970) Fluorescence polarization in immunochemistry. Immunochemistry 7:799–828
114. Van der Molen KL, Klein Koerkamp KJ, Enoch S, Segerink FB, van Hulst NF, Kuipers L (2005) Role of shape and localized resonances in extraordinary transmission through periodic arrays of subwavelength holes: experiment and theory. Phys Rev B 72:045421–1/9
115. Elliott J, Smolyaninov II, Zheludev NI, Zayats AV (2004) Polarization control of optical transmission of a periodic array of elliptical nanoholes in a metal film. Opt Lett 29(12):1414–1416
116. Stewart ME, Anderton CR, Thompson LB, Maria J, Gray SK, Rogers JA, Nuzzo RG (2008) Nanostructured plasmonic sensors. Chem Rev 108:494–521
117. Jin EX, Xu X (2006) Enhanced optical near field from a bowtie aperture. Appl Phys Lett 88:143110–1/
118. Wang L, Uppuluri SM, Jin EX, Xu X (2006) Nanolithography using high transmission nanoscale bowtie apertures. Nano Lett 6(3):361–364
119. Yin L, Vlasko-Vlasov VK, Rydh A, Pearson J, Welp U, Chang S-H, Gray SK, Schatz GC, Brown DB, Kimball CW (2004) Surface plasmons at single nanoholes in Au films. Appl Phys Lett 85(3):467–469
120. Popov E, Neviere M, Wenger J, Lenne P-F, Rigneault H, Chaumet P (2006) Field enhancement in single subwavelength apertures. J Opt Soc Am A 23(9):2342–2348
121. Kim JH, Moyer PJ (2007) Laser-induced fluorescence within subwavelength metallic arrays of nanoholes indicating minimal dependence on hole periodicity. Appl Phys Lett 90:131111–1/3
122. Wenger J, Lenne P-F, Popov E, Rigneault H (2005) Single molecule fluorescence in rectangular nano-apertures. Opt Exp 13(18):7035–7044
123. Rigneault H, Capoulade J, Dintinger J, Wenger J, Bonod N, Popov E, Ebbesen TW, Lenne P-F (2005) Enhancement of single-molecule fluorescence detection in subwavelength apertures. Phys Rev Lett 95:117401–1/4
124. Liu Y, Mahdavi F, Blair S (2005) Enhanced fluorescence transduction properties of metallic nanocavity arrays. IEEE J Sel Top Quantum Electronics 11(4):778–784
125. Samiee KT, Moran-Mirabal JM, Cheung YK, Craighead HG (2006) Zero mode waveguides for single-molecule spectroscopy on lipid membranes. Biophys J 90:3288–3299
126. Levene MJ, Korlach J, Turner SW, Foquet M, Craighead HG, Webb WW (2003) Zero-model waveguides for single-molecule analysis at high concentrations. Science 299:682–868
127. Gryczynski Z, Borejdo J, Calander N, Matveeva EG, Gryczynski I (2006) Minimization of detection volume by surface-plasmon coupled emission. Anal Biochem 356:125–131
128. Gryczynski I, Malicka J, Lakowicz JR, Goldys EM, Calander N, Gryczynski Z (2005) Directional two-photon induced surface plasmon-coupled emission. Thin Solid Films 491:173–176
129. Borejdo J, Gryczynski Z, Calander N, Muthu P, Gryczynski I (2006) Application of surface-plasmon coupled emission to study muscles. Biophys J 91:2626–2635
130. Issa NA, Guckenberger R (2007) Optical nanofocusing on tapered metallic waveguides. Plasmonics 2:31–37

http://www.springer.com/978-3-642-03469-5

Optical Sensor Systems in Biotechnology
Rao, G. (Ed.)
2009, XIV, 162 p. 99 illus., 37 illus. in color., Hardcover
ISBN: 978-3-642-03469-5